UNCERTAINTIES IN ROCK PORE COMPRESSIBILITY AND EFFECTS ON SEISMIC HISTORY MATCHING

A REPORT SUBMITTED TO THE DEPARTMENT OF
PETROLEUM ENGINEERING

OF STANFORD UNIVERSITY

IN PARTIAL FULFILLMENT OF THE REQUIREMENTS FOR THE
DEGREE OF MASTER OF SCIENCE

By
AMIT SUMAN
June 2009

I certify that I have read this report and that in my opinion it is fully adequate, in scope and in quality, as partial fulfillment of the degree of Master of Science in Petroleum Engineering.

Prof. Tapan Mukerji
(Principal Advisor)

Abstract

Seismic history matching involves the use of time-lapse seismic data to match and predict the flow behavior of the reservoir. Time lapse seismic interpretation has evolved as an important diagnostic tool in efficient reservoir characterization and monitoring. Time lapse seismic modeling is an important step in a closed loop history matching where we match flow response as well as time lapse seismic response. The changes in seismic velocities are attributed to changes in saturation and pore pressure, and these velocity changes can be modeled using Gassmann's equations. In this thesis, I explore how uncertainties in mechanical rock properties, specifically rock pore compressibility, can affect the production-related changes in seismic velocities. Reservoir rocks are described by at least four inter-related compressibilities, one of which affects the flow while the other impacts the wave velocities. At first using the Stanford VI synthetic reservoir I show how uncertainties in pore compressibilities can lead to uncertainties in the time-lapse seismic response. Then I extended this idea to a real field where pore compressibilities have been derived from well logs. Using data from Norne field, I have made a rock physics model for elastic properties of different formations. I have presented examples of sensitivity analyses on rock pore compressibility using flow simulation and velocity modeling based on the Norne field dataset. The analyses shows how uncertainties and natural variability in rock pore compressibility, when not accounted for in the flow simulation, can cause pitfalls in modeling of seismic velocities and associated time lapse seismic signatures.

Acknowledgments

First of all, I wish to express my sincere gratitude to my advisor Prof. Tapan Mukerji for his support and guidance without that this research would have been impossible. His consistent guidance and insightful corrections were the catalyst of this research.

I would like to thank the Statoil Hydro Company for providing data on Norne field. I would also like to express my sincere gratitude to Dr. David Echeverria Ciaurri for a detail discussion and critical comments on Norne field dataset. I am highly indebted to the sponsors of Stanford Centre for Reservoir Forecasting (SCRF) group for consistent financial support, and SCRF members for useful discussions.

.

I would like to thanks a ton to the faculty, staff and students of Department of Energy Resources Engineering for their support and contribution to my academic achievements.

Finally, I would like to thank my parents for selfless support, undemanding love and constant motivations.

Contents

List of Tables

List of Figures

Chapter 1

1. Introduction

Seismic time-lapse data has begun to play an important role in reservoir history matching. Time-lapse 3D seismic data can provide information on the dynamics of fluids in the reservoir based on the relation between variations of seismic signals and movement of hydrocarbons and changes in formation pressure. The calibrated reservoir models, optimally constrained to both integrated flow response and spatially distributed seismic responses, will give a better description of the reservoir, and consequently, more reliable forecasts.

Reservoir characterization is based on building and updating a reservoir model by integration of all data available during the different stages of reservoir development. At first an initial static 3D model is built by the integration of seismic data, core and log measurements, and sedimentary models using appropriate geostatistical techniques. This model is used to set up a dynamic model of the reservoir, which allows us to evaluate different possible production scenarios. History matched models are required during the production life of the reservoir to improve forecast reliability. 4-D seismic data i.e. time lapsed 3-D seismic data acquired during production can be used to monitor fluid property changes in the reservoir after specific processing. This new information can be used in the history matching process. Huang et al., (1997, 1998) formulated the simultaneous matching of production and seismic data as an optimization problem, with updating of model parameters such as porosity. Walker and Lane (2007) presented a case study that included time-lapse seismic data as a part of the production history matching process, and show how the use of seismic monitoring can improve reservoir prediction. A typical step in seismic history matching is to compute the effects of changes in saturation and pore pressure on the seismic velocities. Parameters that are updated during history matching include porosity, permeability, and lithology or facies. One of the rock parameters that is often taken to be constant is the rock compressibility with respect to pore pressure. The rock compressibility affects both the flow, and the seismic wave velocities. This work explores the sensitivity of flow response and seismic velocity changes to variations in rock compressibility. What might be some of the pitfalls in time-lapse modeling that might result from ignoring uncertainty in pore compressibility? Section 1.1 defines the various compressibilities used to describe porous media, and how they are related to each other. Chapter 2 describes the overall workflow used in the modeling. In Chapter 3 I present examples of sensitivity analyses using flow simulation and velocity modeling based on the Stanford VI synthetic dataset (Castro et al., 2005).

After that Chapter 4 extends this idea to a real field (Norne field) where pore compressibilities have been derived from well logs. I have used different pore compressibility for different zones derived from rock physics modeling of Norne field based on well log data. I include examples of sensitivity analyses on rock pore compressibility using flow simulation and velocity modeling based on the Norne field dataset. In Chapter 5 conclusions and some future work are outlined.

1.1. Rock and pore compressibility

A nonporous elastic solid has a single compressibility β given by

$$\beta = \frac{1}{V}\frac{\partial V}{\partial \sigma} \tag{1-1}$$

where σ is the hydrostatic stress applied on the outer surface and V is the sample bulk volume. In contrast, compressibilities for porous media are more complicated. We have to account for at least two pressures (the external confining pressure, σ_c and the internal pore pressure, σ_p) and two volumes (bulk volume, v_b and pore volume, υ_p). Therefore, we can define at least four compressibilities. Following Zimmerman's (1991) notation, in which the first subscript indicates the volume change (b for bulk, p for pore) and the second subscript denotes the pressure that is varied (c for confining, p for pore), these compressibilities are

$$C_{bc} = \frac{1}{V_b}\left(\frac{\partial V_b}{\partial \sigma_c}\right)_{\sigma_p} \tag{1-2}$$

$$C_{bp} = \frac{1}{V_b}\left(\frac{\partial V_b}{\partial \sigma_p}\right)_{\sigma_c} \tag{1-3}$$

$$C_{pc} = \frac{1}{\upsilon_p}\left(\frac{\partial \upsilon_p}{\partial \sigma_c}\right)_{\sigma_p} \tag{1-4}$$

$$C_{pp} = \frac{1}{\upsilon_p}\left(\frac{\partial \upsilon_p}{\partial \sigma_p}\right)_{\sigma_c} \tag{1-5}$$

Note that the signs are chosen to ensure that the compressibilities are positive when tensional stress is taken to be positive. Thus, for instance, C_{bp} is to be interpreted as the fractional change in the bulk volume with respect to change in the pore pressure while the confining pressure is held constant. These are the dry or drained bulk and pore compressibilities. The different compressibilities can be related to each other by elasticity theory using linear superposition and reciprocity.

1.2. Closed loop seismic history matching

1.2.1. Flow simulation

The goal of closed loop seismic history matching is to match seismic response as well as flow response of the reservoir at different time during the production history of the reservoir (Figure 1-1). Flow simulation takes in to account the changes in pore volume due to pore compressibility as we produce the reservoir. Note that here I am not considering changes in the porosity due to rock matrix compressibility i.e. geomechanical effects has not been included in this study. Equation 1-6 depicts changes in pore volume due to pore compressibility. $\upsilon(P)$ is the pore volume at specified pressure P and is related with $\upsilon(P_{ref})$ which is the initial pore volume of the reservoir. $\upsilon(P_{ref})$ is calculated based on the initial geometry and porosity of the reservoir.

$$\nu(P) = \nu(P_{ref})(1 + X + \frac{X^2}{2}) \tag{1-6}$$

$$X = C_{pp}(P - P_{ref}) \tag{1-7}$$

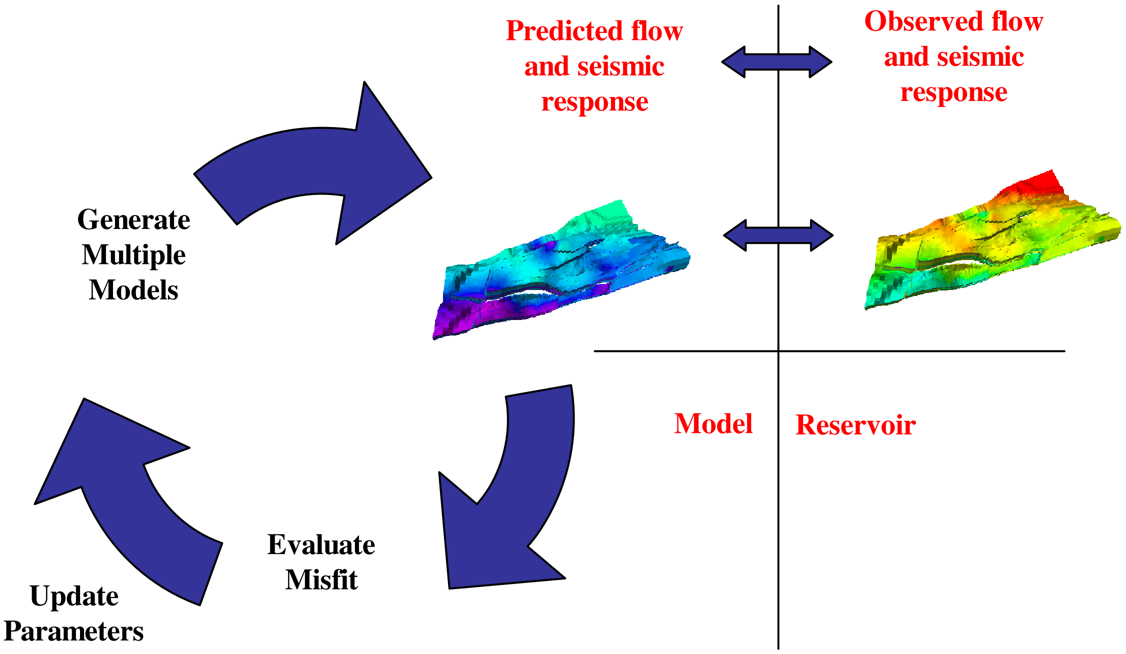

Figure 1-1: Closed loop history matching

1.2.2. Time lapse seismic modeling

The effective dry bulk modulus of the rock is $K_{dry} = 1/C_{bc}$, and is related to the seismic P-wave velocity by $V_P = \sqrt{(K_{dry} + 4G/3)/\rho}$ where ρ is the dry bulk density and G is the shear modulus of the rock. Dry rock velocities can be related to the saturated bulk rock velocity through the Gassmann's equations, described in Chapter 2. The compressibility C_{pp} appears in the fluid flow equations through the storage term, and can be related to C_{bc} (and hence to seismic velocity) by the equation 1-8.

$$C_{pp} = \frac{\left[C_{bc} - (1+\phi)\frac{1}{K_{\min}}\right]}{\phi} \qquad \textbf{(1-8)}$$

where ϕ is the porosity and $K_{\min}$ is the solid mineral bulk modulus.

In time-lapse reservoir modeling the reservoir is often described by a heterogeneous and variable porosity and the seismic velocity is related to variations in saturations and pore pressure. However, the related variability in C_{PP} is not always taken into account. How do variations in this pore compressibility affect the changes in modeled seismic velocities? What might be some of the pitfalls in time-lapse modeling that might result from ignoring uncertainty in C_{PP}? These are the motivating questions that I have begun to address.

Chapter 2

2. Workflow Description

2.1. Rock physics modeling

Rock physics modeling is used in quantitative seismic interpretation to determine the change in elastic properties of rocks due to variations in mineralogy, change in fluid type, variation in saturation and pore pressure and change in the reservoir effective stress. It can also be used to populate acoustic and elastic properties (V_p and V_s and density) inside the reservoir away from the well. Elastic properties (V_p and V_s and density) is calculated at initial condition of the reservoir using available well log data.

2.2. Flow simulation

Flow simulation is performed to generate the inputs required for calculating the 3D seismic velocities (V_p and V_s) at different times during production of the reservoir .Flow simulation provides the saturation of fluids and variation of pore pressure in the reservoir at any particular time and place after the start of production. Saturations of each fluid at every point in space is necessary in order to use Gassmann's equations correctly. To study sensitivity of time lapse seismic modeling on pore compressibility, flow simulation is performed for different cases having different pore compressibilities.

2.2.1. Change in saturation

Flow simulation provides us with the variation of saturation of fluids in the reservoir after the startup of production. As previously stated, seismic velocities are functions of saturations of the different fluids in the reservoir. These variations of saturations are responsible for change in the bulk density, effective bulk elastic moduli, and finally changes in the seismic velocities as shown in the following equations. 3-D time-lapse changes in seismic velocities are generated using initial seismic velocities, density and

Gassmann's fluid substitution equations (Gassmann, 1951) .Gassmann's equation shown below is used to obtain the bulk modulus K_2 of the rock saturated with fluid 2, which is mixture of oil, water and gas in this case.

$$\frac{K_2}{K_{\min}-K_2}-\frac{K_{fl2}}{\phi(K_{\min}-K_{fl2})}=\frac{K_1}{K_{\min}-K_1}-\frac{K_{fl1}}{\phi(K_{\min}-K_{fl1})} \qquad \textbf{(2-1)}$$

K_1 and K_2 are the rock's bulk moduli with fluids 1 and 2 respectively, K_{fl1} and K_{fl2} are the bulk moduli of fluids 1 and 2, φ is the rock's porosity, and K_{min} is the bulk modulus of the mineral. The shear modulus G_2 remains unchanged $G_2 = G_1$ at low frequencies appropriate for surface seismic data, since shear stress cannot be applied to fluids. The fluid bulk moduli are a function of the oil composition, pore pressure and temperature. The fluid moduli and densities are obtained from the usual Batzle-Wang (1992) relations. The density of the rock is also transformed and the density of the rock with the second fluid is computed as:

$$\rho_2=\rho_1+\phi(\rho_{fl2}-\rho_{fl1}) \qquad \textbf{(2-2)}$$

Having transformed the elastic moduli and the density, the compressional and shear wave velocities of the rock with the second fluid are computed as

$$V_p=\sqrt{\frac{K_2+\frac{4}{3}G_2}{\rho_2}} \qquad \textbf{(2-3)}$$

$$V_s=\sqrt{\frac{G_2}{\rho_2}} \qquad \textbf{(2-4)}$$

2.2.2. Change in Pore Pressure

In addition to saturation changes, the elastic moduli of the porous rock frame and hence seismic velocities are affected by pore pressure changes as well. Flow simulation provides us the variation of pore pressure and saturations with respect to time after the startup of the production. Using an appropriate pore pressure model seismic velocities of dry rock are first corrected for changes in pore pressure. Now corrected seismic velocities of dry rocks are used to calculate the seismic velocities by fluid substitution using Gassmann's equation as stated above. The velocity-pore pressure model for the dry rock frame is based on laboratory experiments or empirical relations, appropriate for the type of reservoir rock. Unconsolidated or poorly consolidated rocks in shallow reservoirs are more sensitive to chances in pore pressure.

Chapter 3

3. Stanford VI

In this chapter, the workflow described in Chapter 2 is applied to a synthetic dataset to test the sensitivity of variations in pore compressibility on the results of seismic time lapse modeling.

3.1. Geology

Stanford VI (Castro et al., 2005) is an exhaustive synthetic data set. It has structure of an anticline. The anticline is asymmetric with axis N15˚E. It has different dips on each flank and the dip decreases slowly towards the northern part of the structure. The maximum dip of the structure is 8° (Figure 3-1).

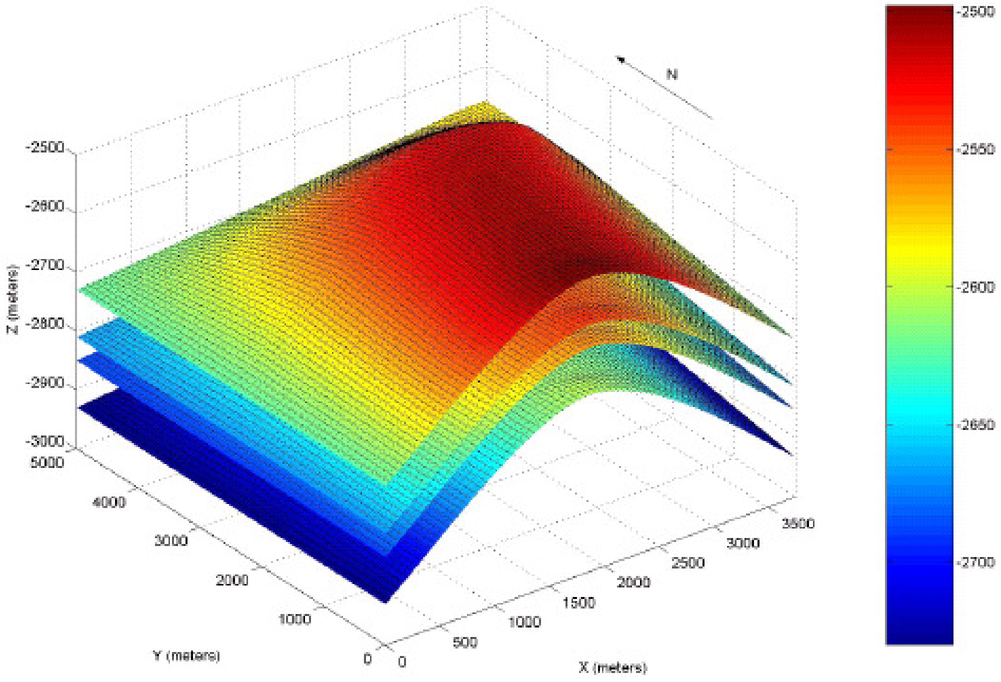

Castro, 2005

Figure 3-1: Horizons of Stanford VI: presence of an anticline in N15˚E

The reservoir is 5.0 Km long (North-South) and 3.75 Km wide (East-West). It has a depth range of 2.5 Km to 2.7Km. The reservoir has thickness of 200m and consists of three layers with thicknesses of 80 m, 40 m and 80 m respectively. The original reservoir model is represented in a 3D regular grid of 6 million cells (150 x 200 x 200), with realistic dimensions (25m in the X and Y directions and 1m in the Z direction).

The stratigraphic model corresponds to a fluvial channel system, and the petrophysical properties computed for this reference reservoir correspond to the classical porosity, density, permeability and seismic P-wave and S-wave velocities. The first layer consists of a system of channels made by four facies: the floodplain (shale deposits), the point bar (sand deposits), and the channel (sand deposits), and the boundary (shale deposits). The second layer consists of meandering channels also represented by four facies: the floodplain (shale deposits), the point bar (sand deposits), and the channel (sand deposits), and the boundary (shale deposits). The last and third layer of the reservoir consists of deltaic deposits and are represented by two facies: the floodplain (shale deposits), and the channel (sand deposits).

3.2. Data available

Seismic P-wave and S-wave velocities are available at initial condition of the reservoir. These seismic attributes are generated at point support using rock physics expressions. For this study the original reservoir model is upscaled such that new upscaled model approximately preserves the local heterogeneities. The model used for this study has 0.75 million cells (75x100x100) with appropriate dimension (50m in X and Y direction and 2m in Z direction). Since initial seismic attributes were already available so there was no need of rock physics modeling for Stanford VI. Rock physics models were already used by Castro et al. (2005) to generate the synthetic data. The reservoir is produced for thirty years with thirty producers and fifteen water injectors.

3.3. Flow simulation

Flow simulation is performed to generate the inputs required for calculating 3D seismic velocities (V_p and V_s) at different times during oil production. Water and oil are the only fluids present in the reservoir. We have used an isothermal black-oil model because reservoir has only two phases (oil and water) and water is injected at a certain time during the flow simulation. Thirty years of oil production have been simulated. There is an active aquifer below the reservoir and water injector wells become active after the aquifer water influx fails to maintain the pressure. Flow simulation is performed for two different cases having different pore compressibilities. Case I and case II have pore compressibility (C_{pp}) of 1e-5 psi^{-1} and 1e-6 psi^{-1} respectively.

Table 3-1 shows oil and water PVT properties used for the flow simulation. The relative permeability curves are constant in the flow simulation. No capillary pressure is considered in the flow simulation.

Property	Oil	Water
Density (lb/ft^3)	45.09	61.80
Viscosity (cp)	1.18	0.325
Formation Volume Factor	0.98	1.0

Table 3-1: Fluid properties for flow simulation

Water-oil contact is at the depth of 9, 840 ft. The constant water inflow rate from aquifer is of 31, 000STB/day. The reservoir is produced for 30 years with 31 oil producer wells and 15 water injector wells. The flow simulation starts with only six wells in production. and new wells are constantly added . Producer wells have constant liquid rate production and BHP constraint of 2700psia. Injector wells have constant water injection rate.

3.4. Time lapse seismic modeling

Time lapse seismic modeling is performed to calculate seismic velocities at ten, twenty and thirty years after production of reservoir. At first seismic velocities are obtained taking in to account only saturation changes as described in Chapter 2. Then seismic velocities are calculated considering effect of pore pressure changes on dry rock frame as well as change of saturation. The pore pressure effect on the dry rock frame in Stanford VI is modeled using an exponential relation, based on an empirical relation derived from dry core data for Gulf of Mexico sandstones (Avseth et al., 2005) (Figure 3-2).

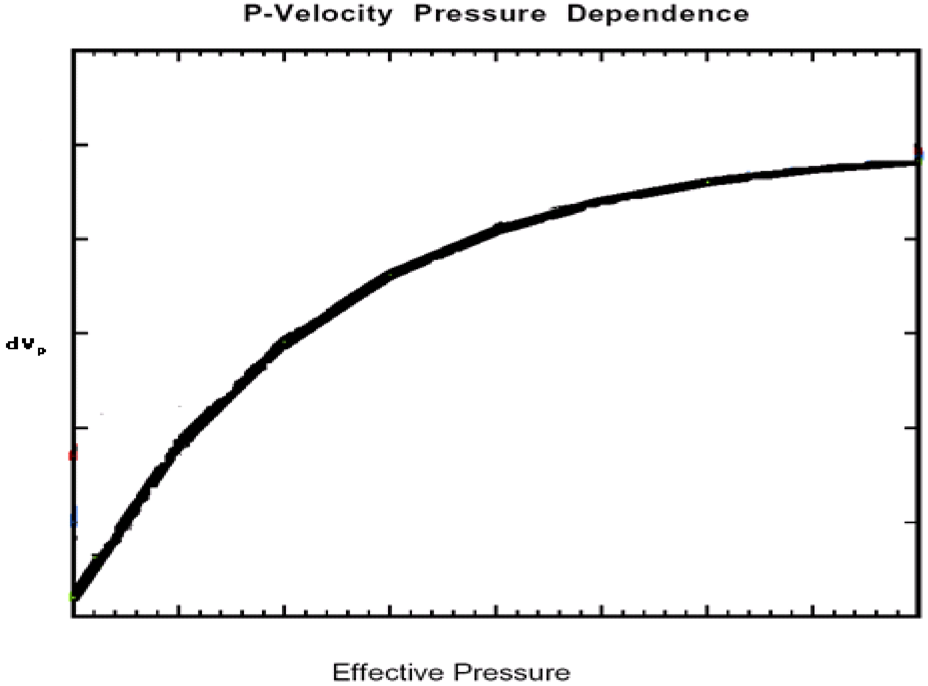

Figure 3-2: Change in seismic velocity due to pore pressure in Stanford VI

3.5. Results

All of the figures below show V_p at different times at different cross section of a Cartesian grid. The results are shown on a Cartesian grid having the same I, J, and K as that of reservoir model. Figure 3-3 shows V_p at the initial condition of the reservoir. Figures 3-4, 3-5 and 3-6 show the percentage change in V_p after 10, 20 and 30 year of production respectively for case I. These results only consider the changes in saturation with respect to time. So far we have not considered the effect of change of pore pressure on the dry rock frame.

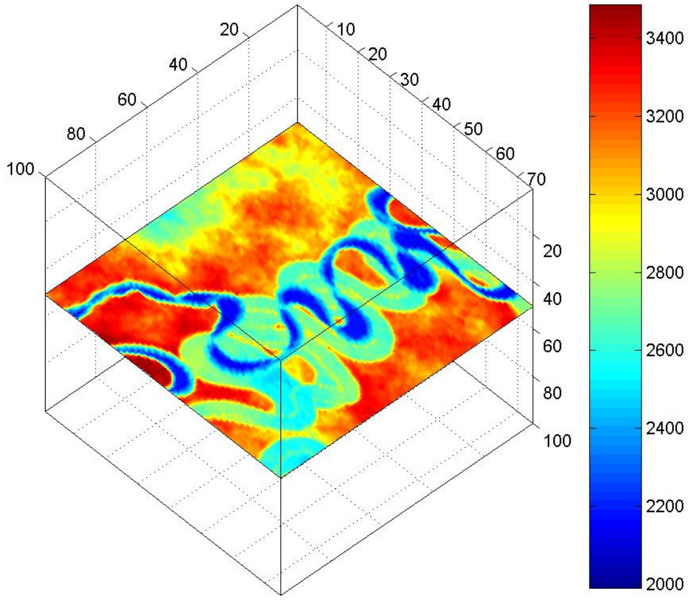

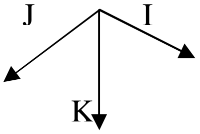

Figure 3-3: V_p at Initial Reservoir condition at K = 50

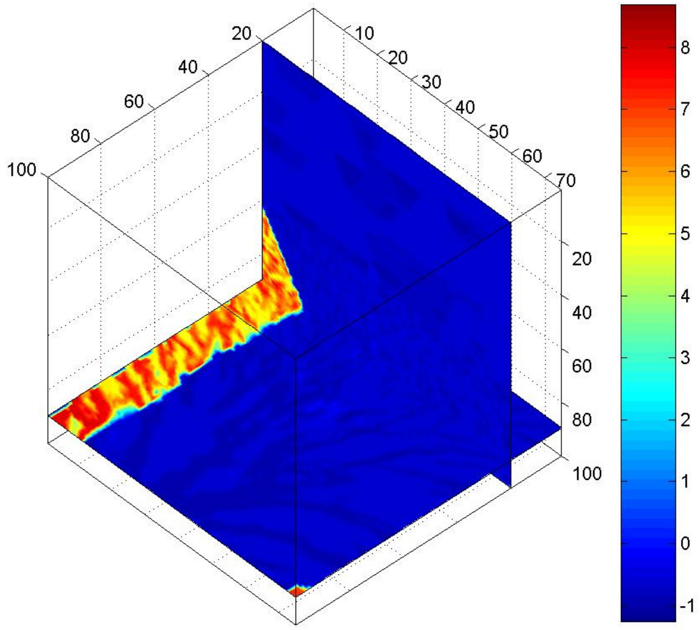

Figure 3-4: Percent change in V_p after 10 years

–

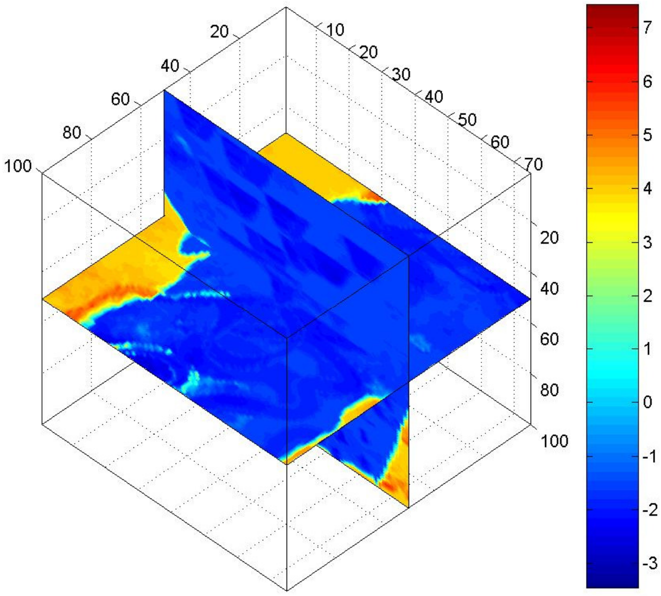

Figure 3-5: Percent change in V_p after 20 years

–

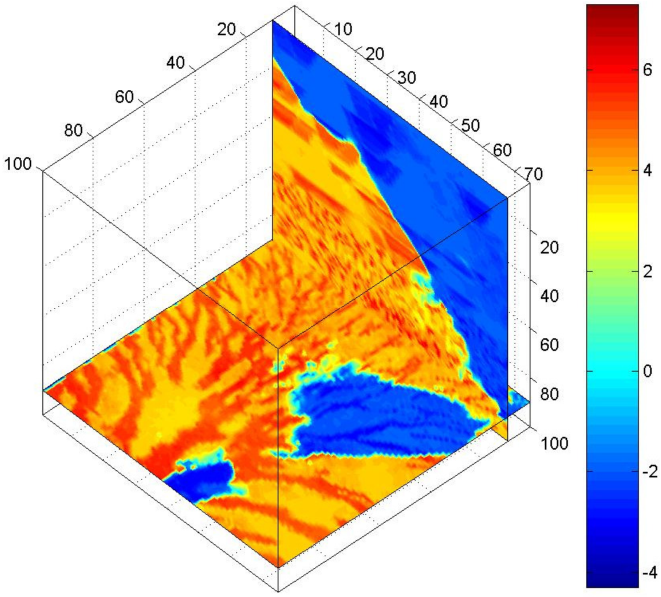

Figure 3-6: Percent change in V_p after 30 years

There are no significant variations in the saturation distribution for two different compressibilities. As a result, there is no significant variation in the seismic wave velocities for two different values of pore compressibilities. Maximum percentage change in V_p is around 6 % - 7 % and it is almost the same for both the compressibilities.

Our next step is to consider the effect of change of saturation as well as changes in pore pressure on seismic velocities, since the effect of uncertainty in C_{PP} impacts mostly the pore pressure distributions. Figures 3-7 to 3-12 show V_p for two different pore compressibility after 10, 20 and 30 year of production. Figures 3-13 to 3-18 show percentage change in V_p after 10, 20 and 30 year of production.

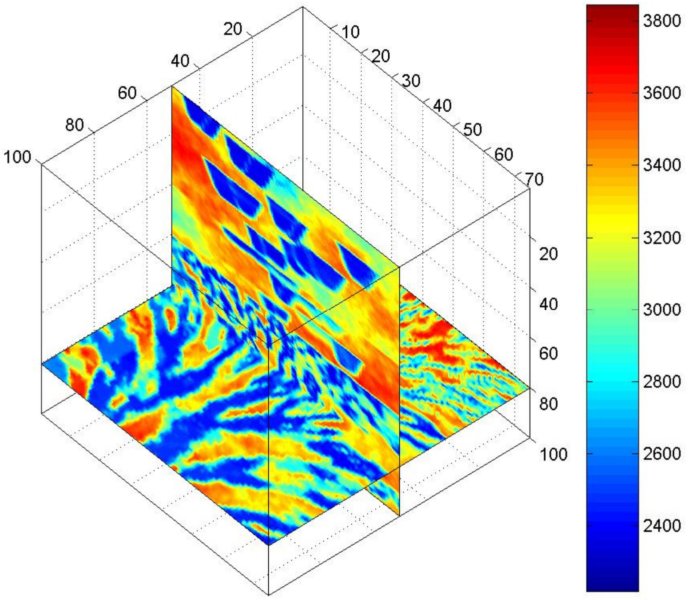

Figure 3-7: V_p after ten years in Case I

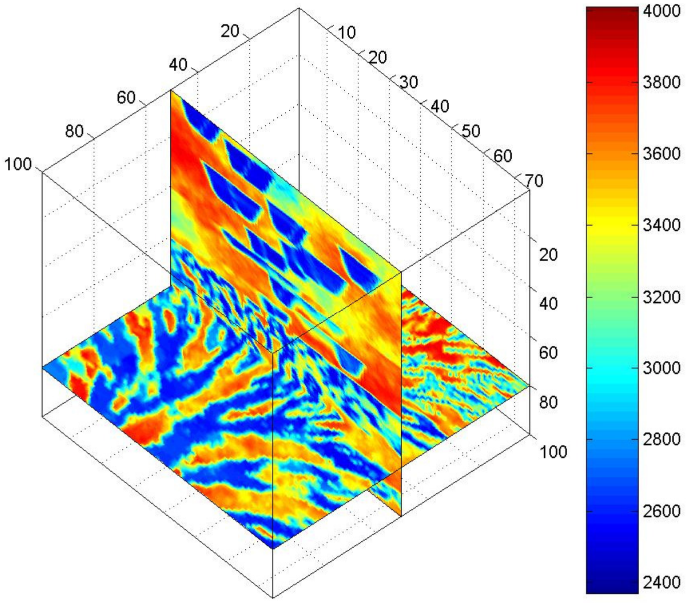

Figure 3-8: V_p after ten years in Case II

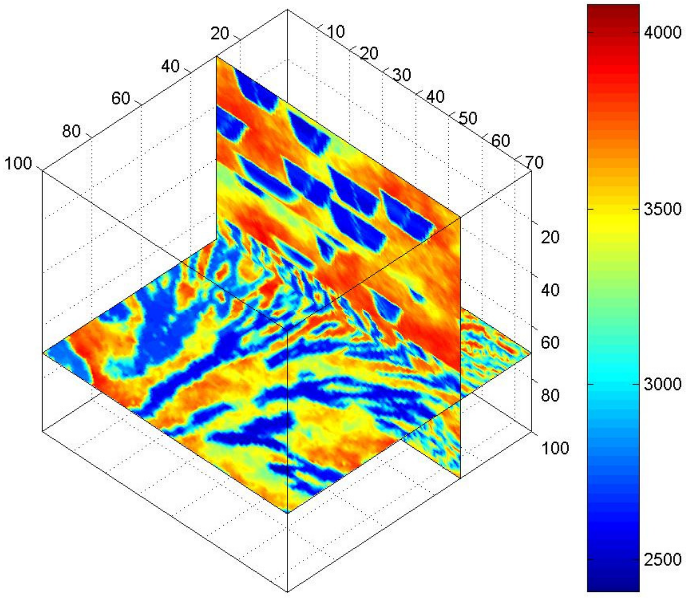

Figure 3-9: V_p after twenty years in Case I

–

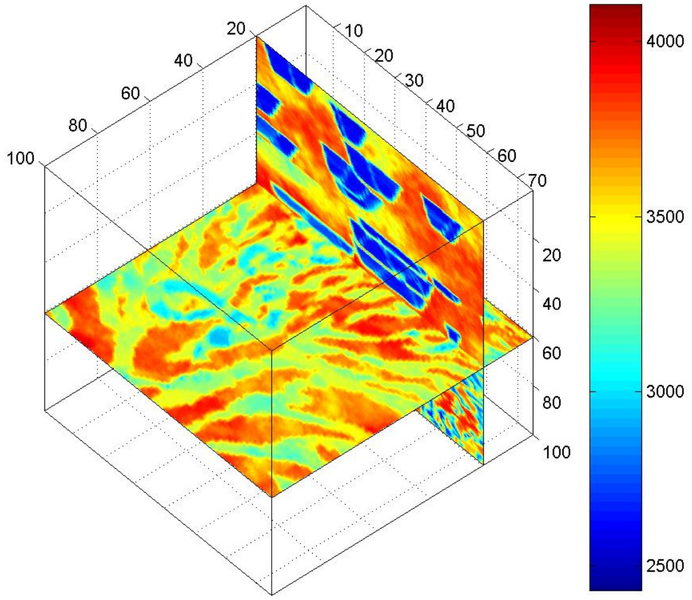

Figure 3-10: V_p after twenty years in Case II

–

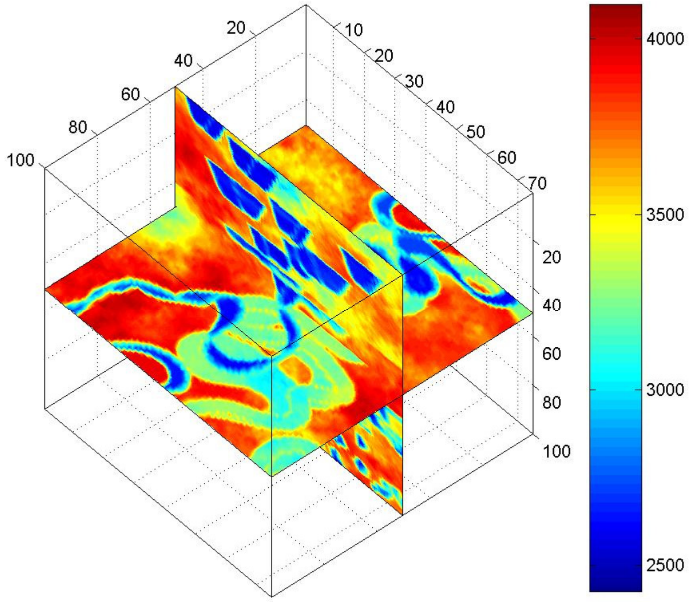

Figure 3-11: V_p after thirty years in Case I

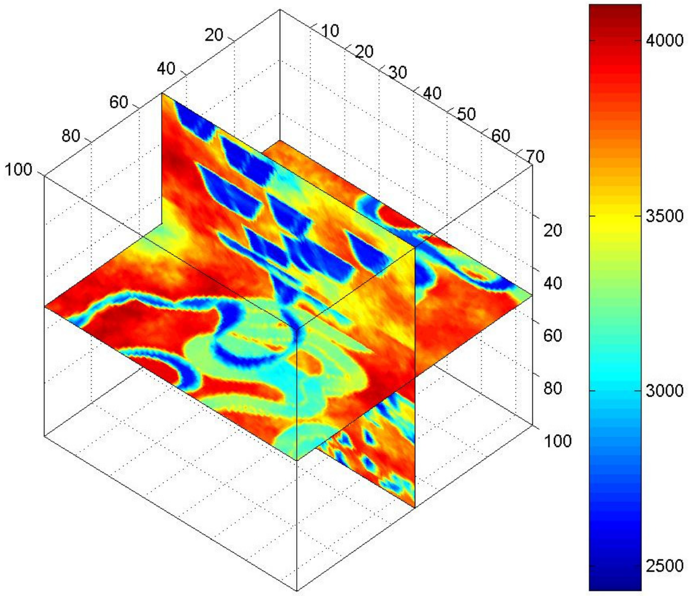

Figure 3-12: V_p after thirty years in Case II

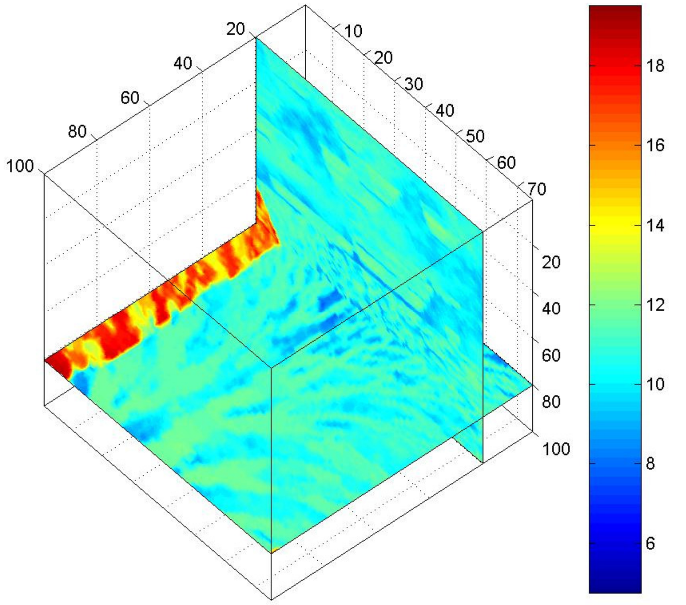

Figure 3-13: % Change in V_p after 10 years in Case I

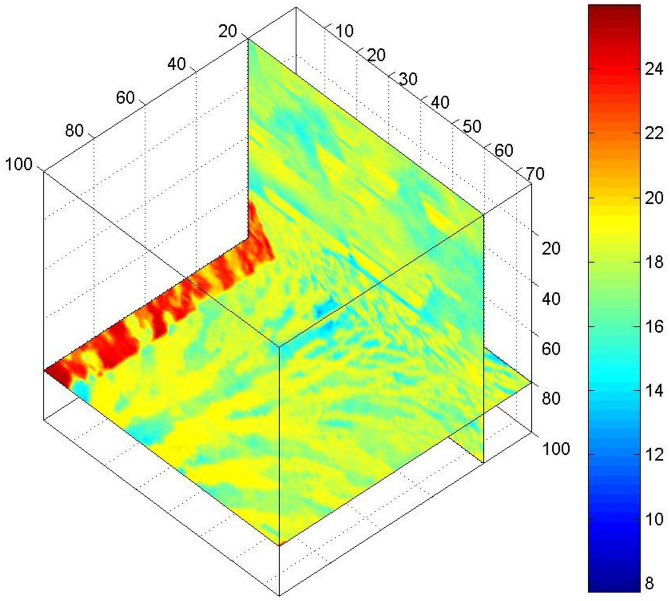

Figure 3-14: % Change in V_p after 10 years in Case II

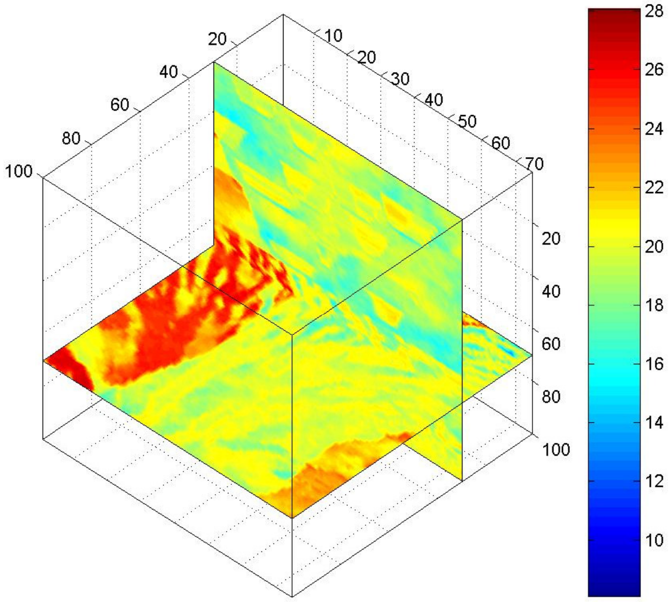

Figure 3-15: % Change in V_p after 20 years in Case I

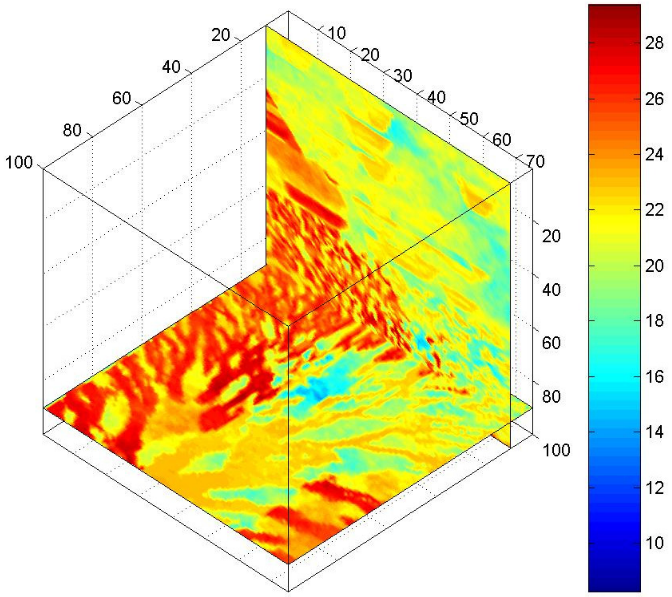

Figure 3-16: % Change in V_p after 20 years in Case II

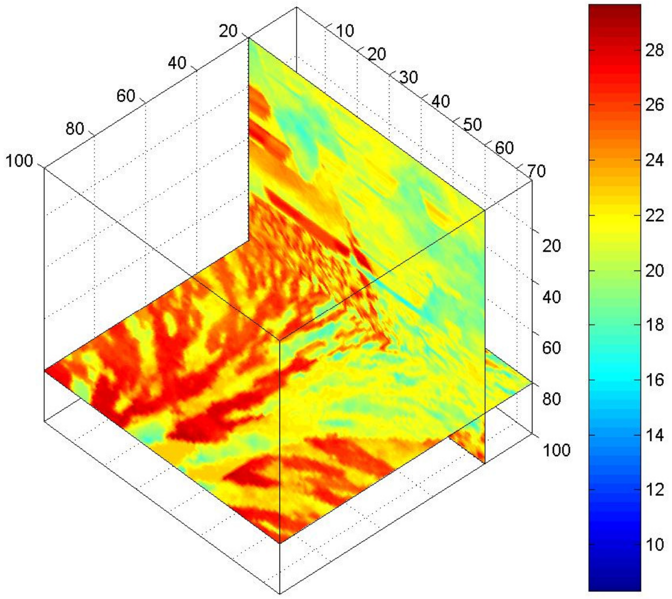

Figure 3-17: % Change in V_p after 30 years in Case I

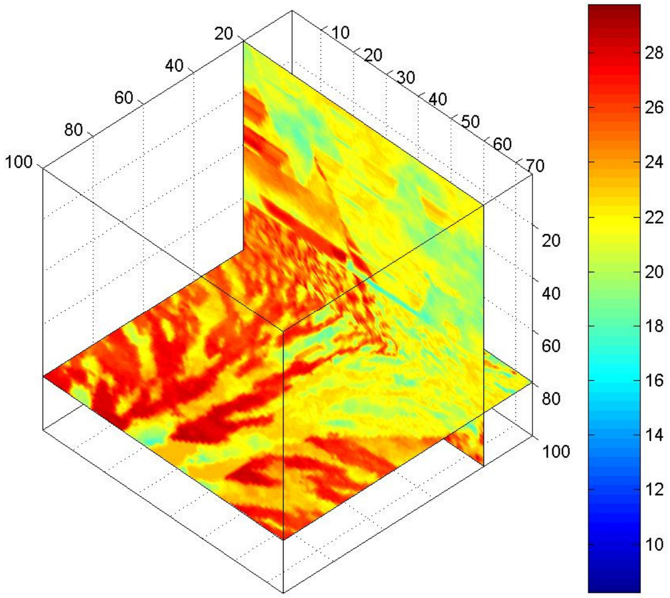

Figure 3-18: % Change in V_p after 30 years in Case II

We observe a significant increase in % change of V_p. The maximum % change in V_p after 10 years due to saturation change is 6%-7%. Now when we consider in addition the effect of change of pore pressure the maximum % change in V_p is 17%-18% after 10 year of production for pore compressibility of 1e-5 psi^{-1}. For pore compressibility of 1e-6 psi^{-1} the maximum % change in V_p after 10 year of production is 24%-25%. Therefore, for two different pore compressibilities the difference in maximum % change in V_p is around 6%-7%. In addition, the differences are significant as compared to the previous case where only saturation effects were considered. These observations indicate that production-related changes in seismic velocities can depend upon pore compressibility and thus uncertainties attached to pore compressibilities can not be ignored in time-lapse modeling. There is an increase in % change in V_p after 20 years and 30 year of production but it is very similar for both the pore compressibilities. This is because injectors come into play maintaining the pore pressure. Thus, changes in pore pressure and pore compressibility play an important role in time-lapse modeling and hence in seismic history matching.

These are very preliminary observations based on a synthetic model, and further analysis on the variation of pore compressibilities, and their relation to different lithologies are needed. The effect of different rock compressibility on seismic history matching is an important issue and should be studied in detail. In the following Chapter we will see the results for Norne field.

Chapter 4

4. Norne field

The Norne field is located in the blocks 6608/10 and 6508/10 on a horst block in the southern part of the Nordland II area in the Norwegian Sea. The horst block is approximately 9 km x 3 km. It has 29 producer and 10 injector wells. The present geological model consists of five reservoir zones. They are Garn, Not, Ile, Tofte and Tilje (Figure 4-1).

4.1. Geology

The Tilje formation was deposited in a marginal marine, tidally affected environment. Sediments deposited are mostly sand with some clay and conglomerates. An unconformity is discovered at the top of the Tilje formation. It has a heterolithic composition consisting of sandstone layers of variable thickness, heavily bioturbated shales, laminated shale and conglomeratic beds.

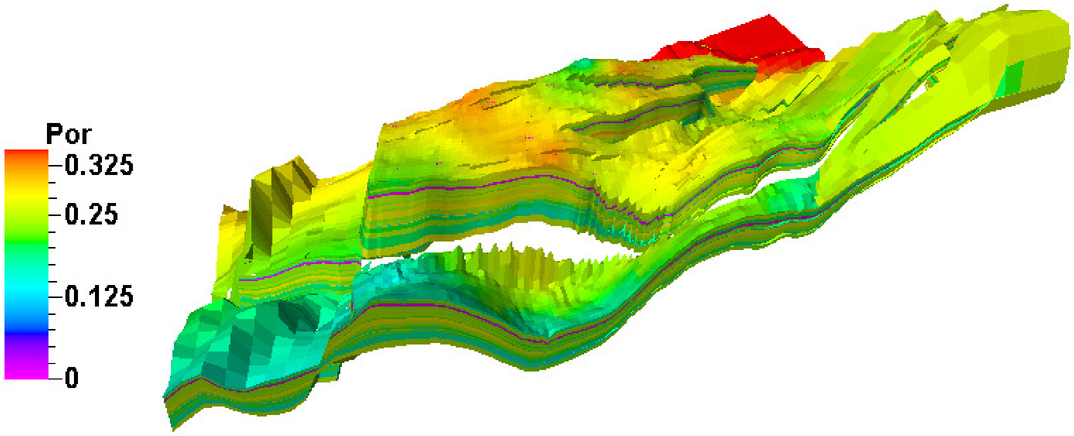

Figure 4-1: Structure of Norne field. Garn has highest porosity

The Tofte formation was deposited on top of the unconformity mentioned above during the Late Toracian. Mean thickness of the Tofte formation across the field is 50 m. It consists of medium to coarse grained sandstones with steep dipping lamina. The lower parts are more bioturbated and have finer grains.

The Ile formation was deposited during the Aalenian, and is 32-40 thick sandstone. The reservoir quality of the Ile formation is generally good, especially in the regressive deposition, whereas the reservoir properties are decreasing toward the top of the formation.

The Not formation was also deposited during Aalenian time. It is a 7.5 m thick, dark grey to black claystone with siltstone lamina. The depositional environment was quiet marine, probably below wave base. It has a coarsening upward trend.

The Garn formation was deposited during the Late Aalenian and is 35 m thick sandstone. The depositional environment was near shore with some tidal influence. Reservoir quality is increasing upward within the formation, from pretty good in the lower parts to very good in the upper parts. The upper part is a sandstone unit which is coarsening upward from very fine to the fine grained sand. The lower part is muddy and bioturbated, as it is the continuance of the Not formation, while the upper part has an increased sand content.

4.2. Data available

Well log data is available for each of the wells. Well logs of nine different wells have been considered for this study. These logs consist of porosity, volume of shale, saturations, sonic log and density. Well log data are analyzed for relationships among Vp, Vs, porosity, density and lithology. These relationships vary across different zones and therefore each geological setting is characterized individually.

The reservoir model is represented in a 3D regular grid of 113344 cells (46 x 112 x 22) (122 m, 129 m, 8.5 m) Petrophysical properties available for this model are porosity, permeability and net to gross ratio. The zonation is made to correspond as much as possible to the actual change of lithology in the layers of the reservoir. Hence, boundaries between zones are chosen at sequence boundaries and maximum flooding surfaces.

Lithological boundaries and distinct breaks in porosity or permeability that correlate across the field can also be basis for the zonation. Oil is mainly found in the Ile and Tofte Formations, and gas in the Garn formation. The sandstones are buried at a depth of 2500-2700 m. The porosity is in the range of 25-30 % while permeability varies from 20 to 2500 mD (Steffensen and Karstad, 1995; Osdal et al., 2006).

4.3. Pore Compressibility

Pore compressibility for each of the zone is calculated based on the well log data and using the relation between C_{pp} and C_{bc} as described in Chapter 1. In order to do this, first Gassmann's equation is used to transform the log sonic velocities to dry conditions. Then, the velocities are converted to bulk rock compressibilities C_{bc}. Figure 4-2, 4-3, 4-4 and 4-5 shows histograms of pore compressibility C_{pp} in each of the zones. The plots show that the pore compressibility can vary within formations by factors of 2 to 4 and by an order of magnitude across different formations. Yet, often in flow simulations (typically simulations that do not account for geomechanics) though porosity is taken to vary over every grid block, the corresponding rock pore compressibility is taken to be a constant. This is clearly an inconsistent model. Pore compressibility of the rock varies with porosity in each of the zones in Norne and shown in the figure 4-6, 4-7, 4-8 and 4-9. But is it important to take into account the variability in the pore compressibility? How does the variability in pore compressibility affect the computed saturations and pressures, and the computed time lapse changes in seismic signatures?

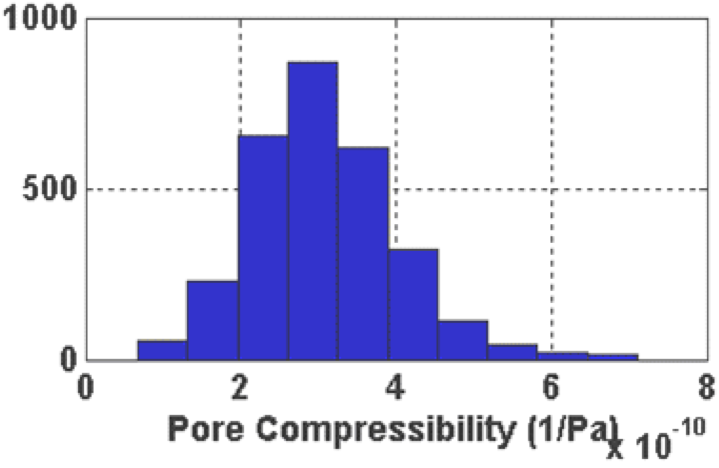

Figure 4-2: Histogram of pore compressibility in GARN

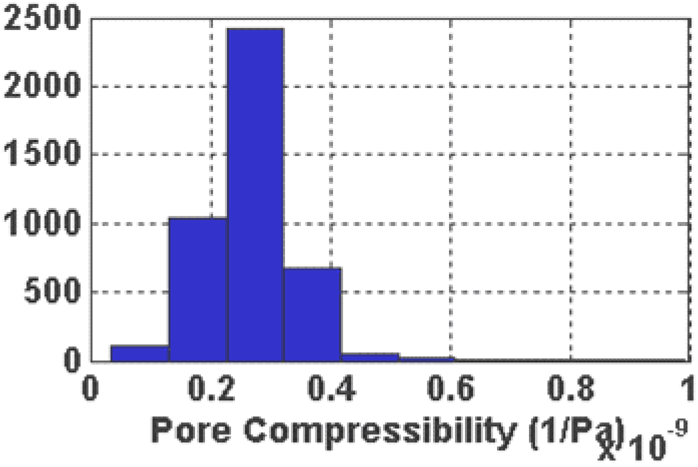

Figure 4-3: Histogram of pore compressibility in ILE

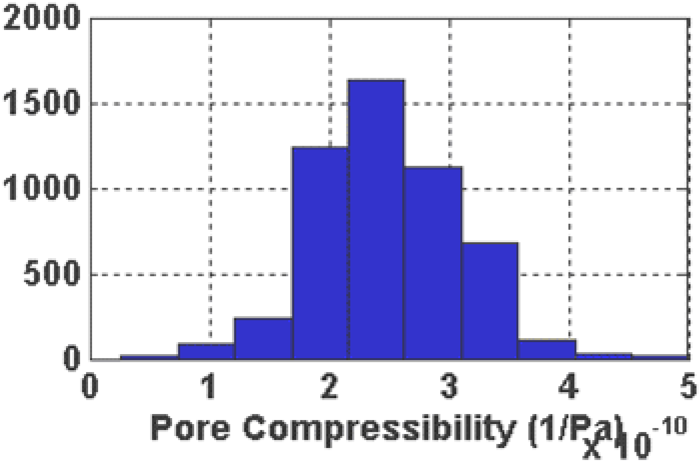

Figure 4-4: Histogram of pore compressibility in TOFTE

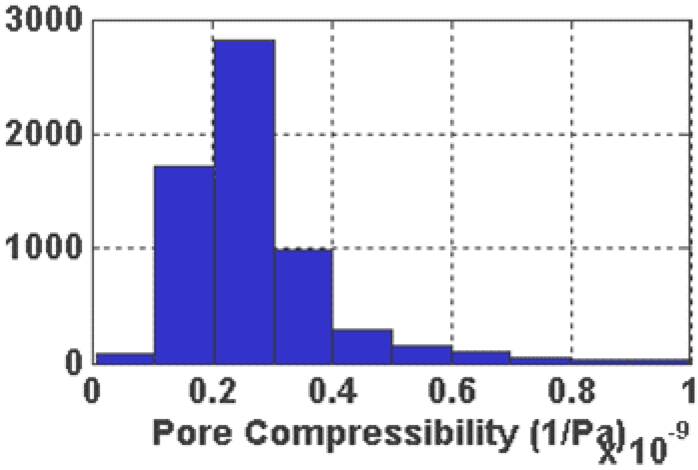

Figure 4-5: Histogram of pore compressibility in TILJE

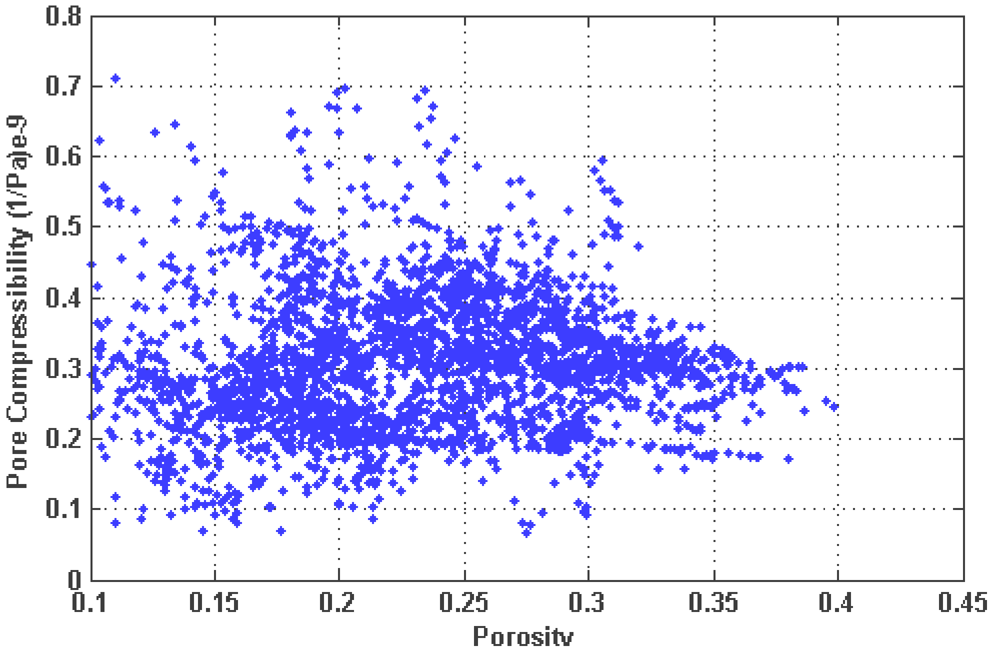

Figure 4-6: Variation of C_{PP} with porosity in GARN

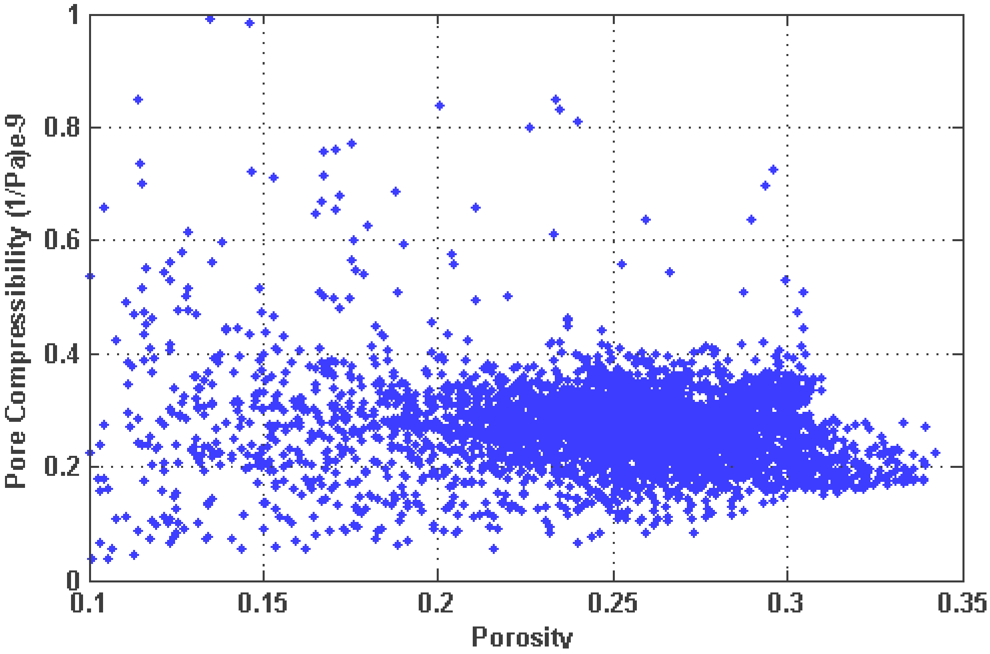

Figure 4-7: Variation of C_{PP} with porosity in ILE

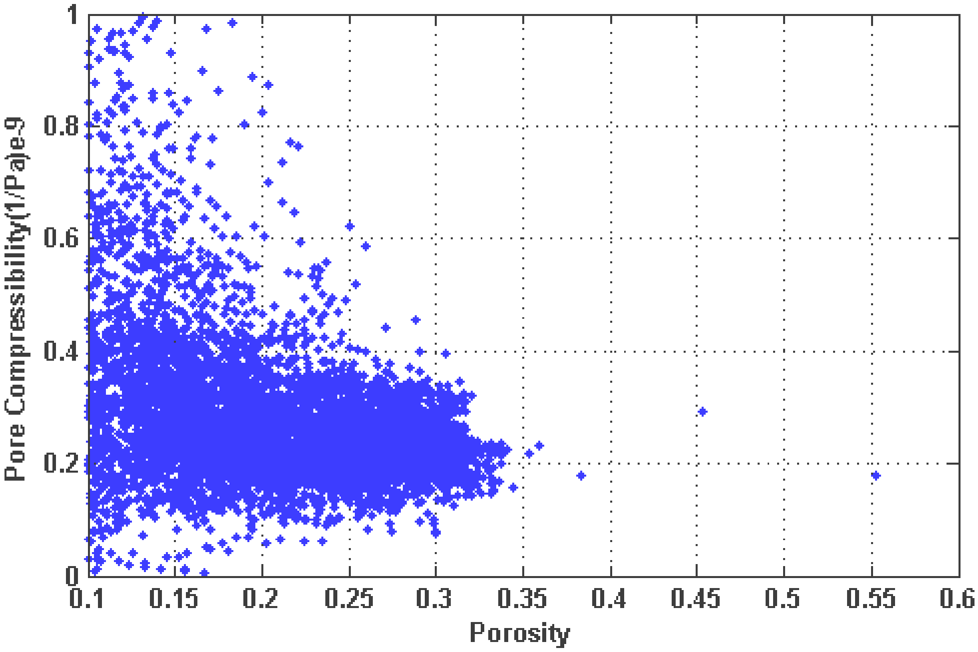

Figure 4-8: Variation of C_{PP} with porosity in TILJE

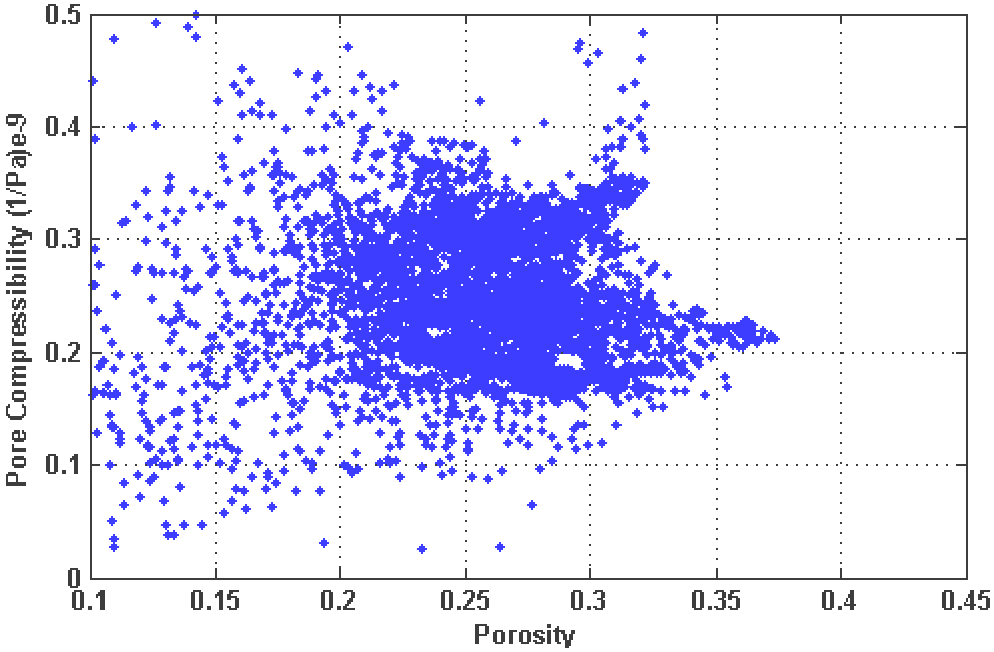

Figure 4-9: Variation of C_{PP} with porosity in TOFTE

4.4. Rock physics modeling

The basis of our approach is to relate elastic moduli and porosity near the well (based on the well log data) and use this relation to populate the reservoir model away from the well. Elastic properties of Norne field at initial condition have been established using available well log data.

4.4.1. Dvorkin's unconsolidated sand model

Dvorkin's unconsolidated sand model (Dvorkin et al., 1996) is used which relates the elastic moduli of high porosity sediments to porosity, mineralogy and effective pressure. Hertz-Mindlin contact theory is used to calculate the effective bulk and shear moduli of the rock frame at the critical porosity. Bulk and shear moduli of the rock frame having porosity below critical are calculated using the modified lower Hashin-Shtrikman bound. Using Hertz-Mindlin contact theory effective bulk moduli (K_{HM}) and effective shear moduli (G_{HM}) at critical porosity are calculated as follows:

$$K_{HM} = \left[\frac{C^2 (1-\phi_0)^2 G^2}{18 \pi^2 (1-\nu)^2} P \right]^{1/3} \qquad \textbf{(4-1)}$$

$$G_{HM} = \frac{5-4\nu}{5(2-\nu)} \left[\frac{3C^2 (1-\phi_0)^2 G^2}{2\pi^2 (1-\nu)^2} P \right]^{1/3} \qquad \textbf{(4-2)}$$

Where C is the average number of contacts per grain, υ is the Poisson's ratio of the solid grain, G is the grain shear modulus and P is the hydrostatic pressure. These moduli at critical porosity are then used as inputs to compute the effective moduli at other porosities using a heuristic modified Hashin-Strikman lower bound as follows:

$$K_{eff} = \left[\frac{\phi / \phi_0}{K_{HM} + \frac{4}{3} G_{HM}} + \frac{1 - \phi / \phi_0}{K + \frac{4}{3} G_{HM}} \right]^{-1} - \frac{4}{3} G_{HM} \qquad \textbf{(4-3)}$$

$$G_{eff} = \left[\frac{\phi/\phi_0}{G_{HM} + \frac{G_{HM}}{6} \left(\frac{9K_{HM} + 8G_{HM}}{K_{HM} + 2G_{HM}} \right)} + \frac{1-\phi/\phi_0}{G + \frac{G_{HM}}{6} \left(\frac{9K_{HM} + 8G_{HM}}{K_{HM} + 2G_{HM}} \right)} \right]^{-1} - \frac{G_{HM}}{6} \left(\frac{9K_{HM} + 8G_{HM}}{K_{HM} + 2G_{HM}} \right) \qquad \textbf{(4-4)}$$

Well log sonic data (both compressional and shear) and the density log can be used to extract the bulk and shear moduli of the rocks. These moduli correspond to different states of pore fluid saturation. In order to fit a rock model, all data have to be transformed to a uniform reference saturation. Using Gassmann's equation all the moduli near the well is calculated for 100% brine saturation. Based on the moduli and porosity we come up with a rock physics model for elastic moduli versus porosity near the well. Once we have the model for near the well then based on the porosity values in the reservoir simulation model away from the well we calculate moduli for each of the zones. Finally we get distribution of V_P and V_S for the whole reservoir. Figure 4-10 provides an overview of rock physics modeling procedure described above. Rock physics modeling of each of the zones is described in the following section.

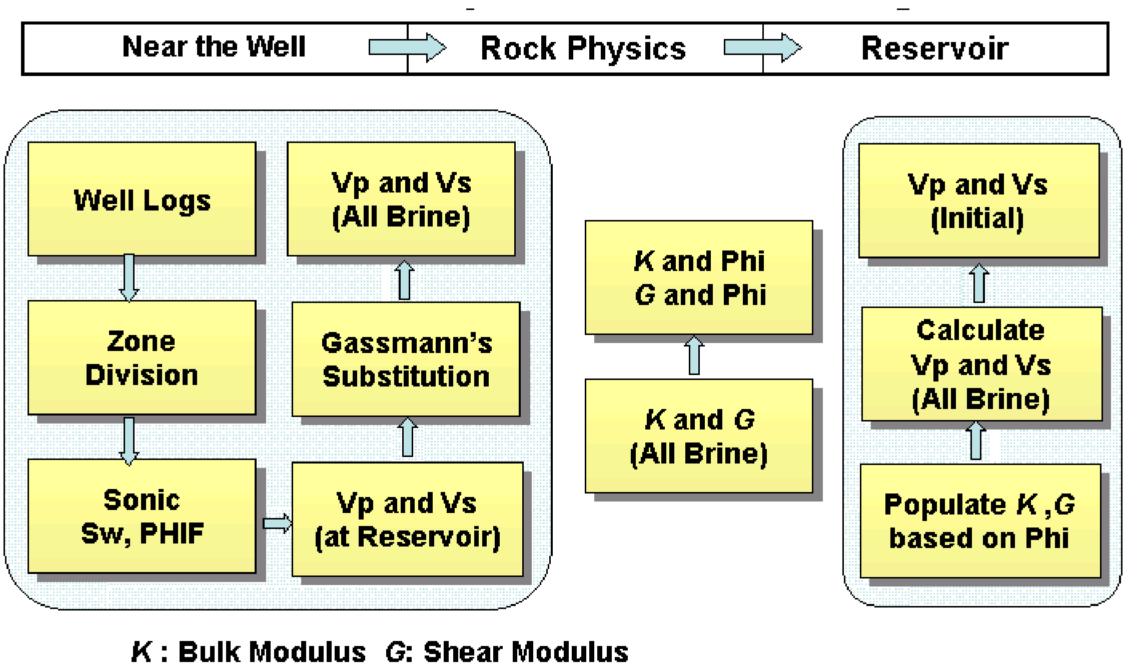

Figure 4-10: Rock physics modeling procedure, from well data to model

4.4.2. GARN Formation

Figure 4-11 shows a plot of bulk modulus and porosity near the well inside the Garn formation. Color bar indicates depth of the data points in the garn formation. Colors of the data points indicate that all the data points are in depth range of 2540-2700 m. The plot shows two depth trends. First trend is for the data points above 2600m and second is for below 2600m. These depth trends have been modeled using the unconsolidated sand model.

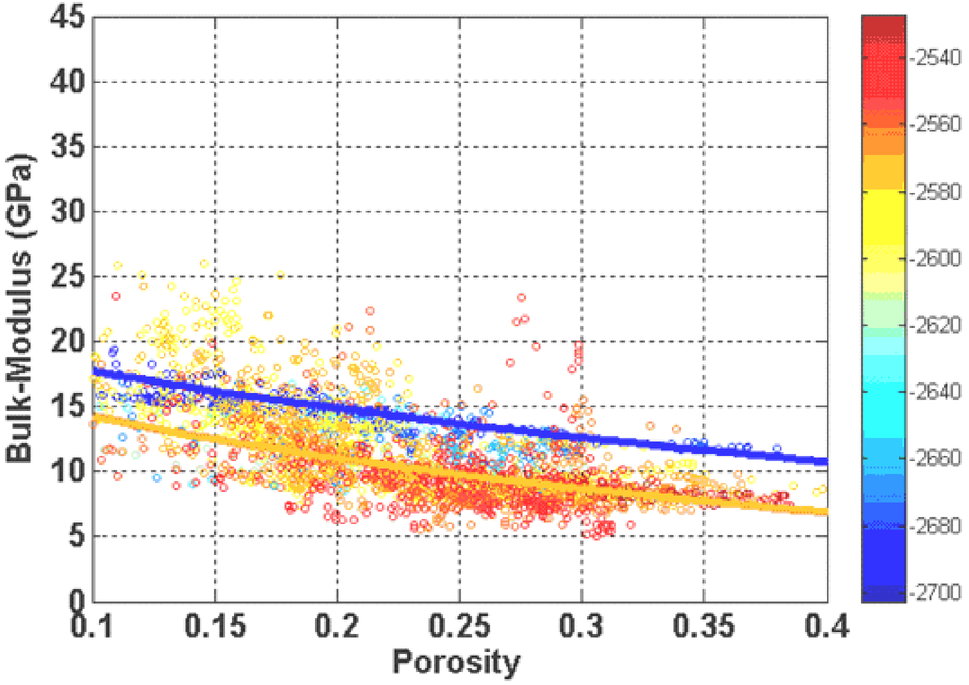

Figure 4-11: Two depth trends in Garn formation

4.4.3. TOFTE Formation

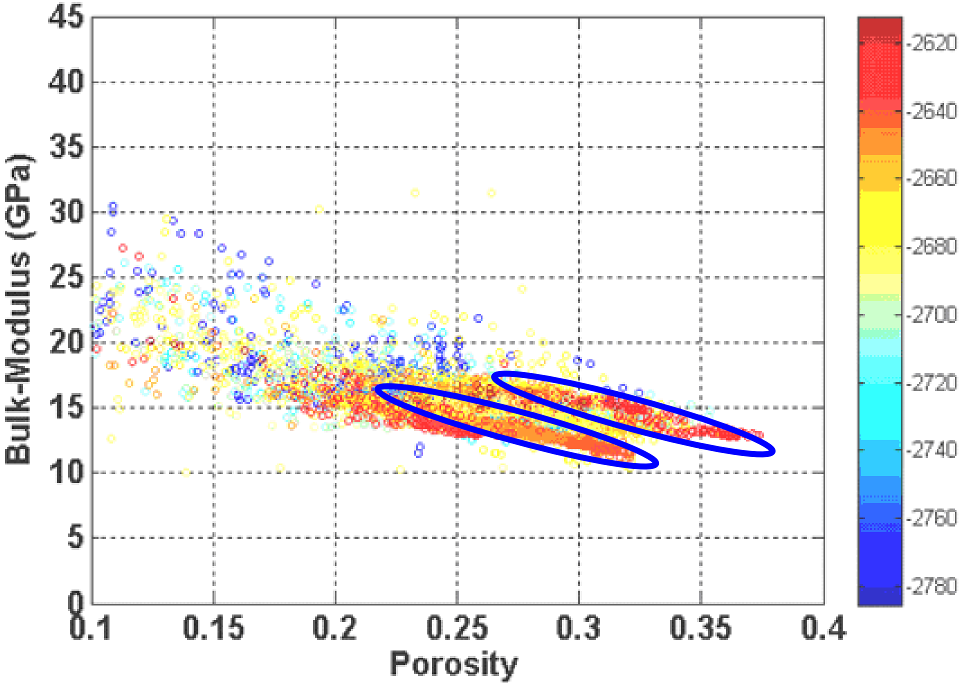

Figure 4-12: Two trends in Tofte but at the same depth

Figure 4-12 indicates two trends in the data set of TOFTE formation. Both the trends are for same depth ranges, but from different sections of the reservoir. There are three main faults inside the reservoir as shown in the figure 4-13. The data points corresponding to trends in the figure 4-12 above belongs to different sections in the reservoir separated by faults. These faults separate reservoir in four different sections and further analysis is based on four different regions in each of the zones. A clear trend has been established in each of the faulted regions in TOFTE as shown in the figures 4-14, 4-15, 4-16 and 4-17.

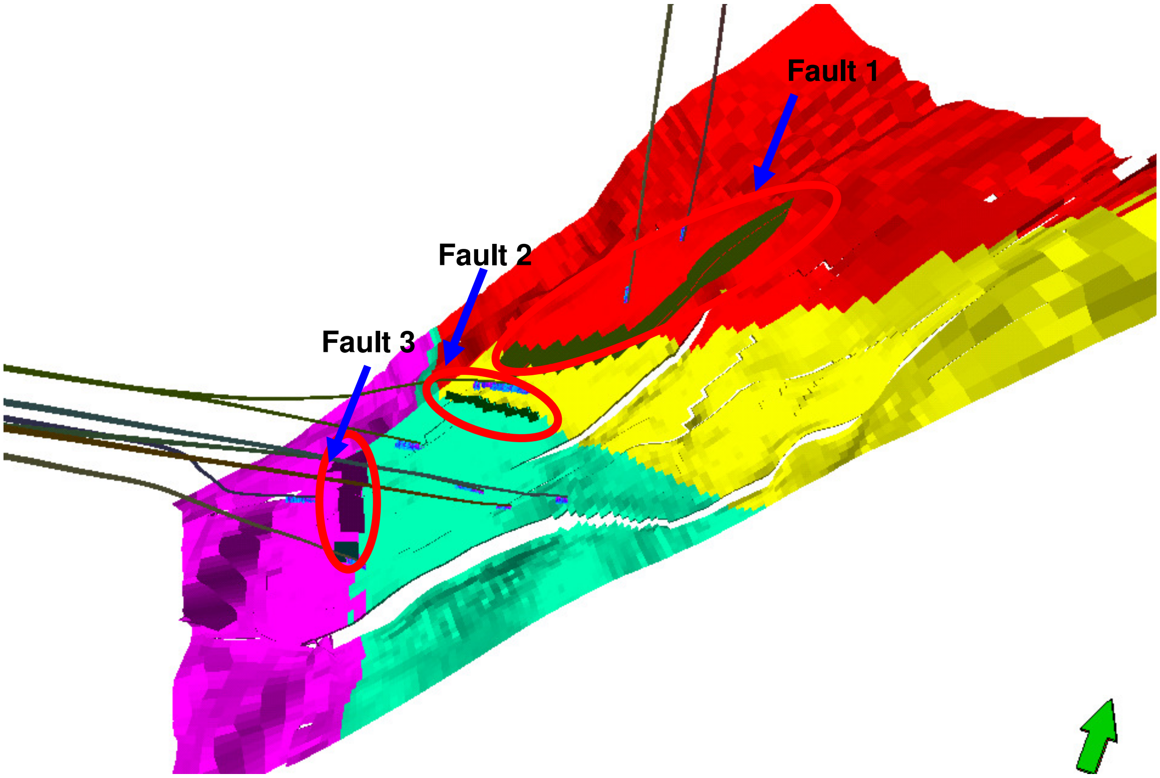

Figure 4-13: Three main faults, four regions and well clustering in Norne field

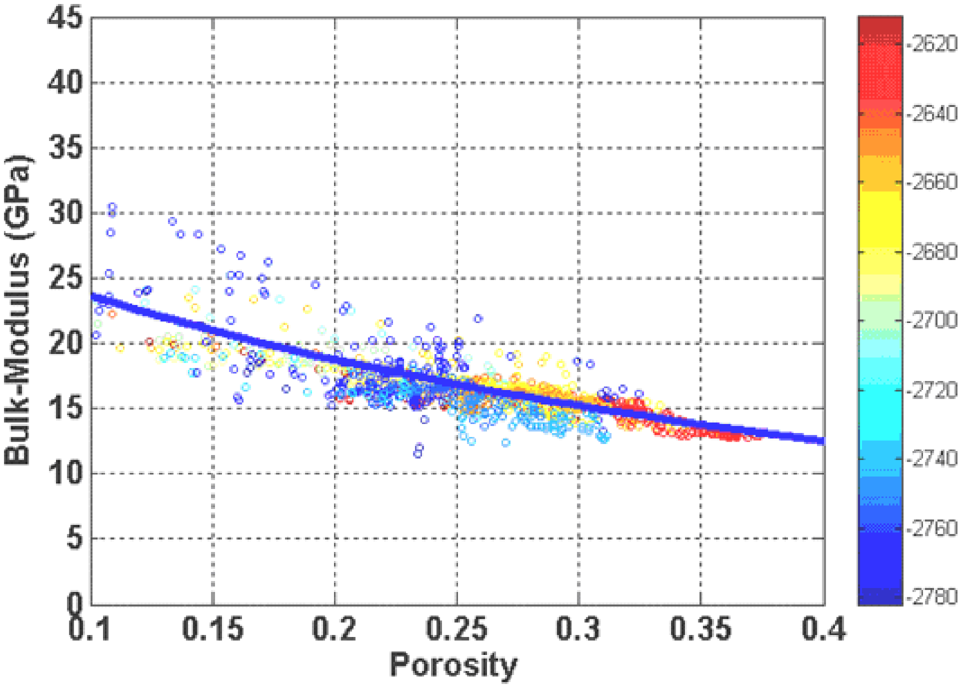

Figure 4-14: Bulk-modulus versus porosity model of TOFTE (Region 1)

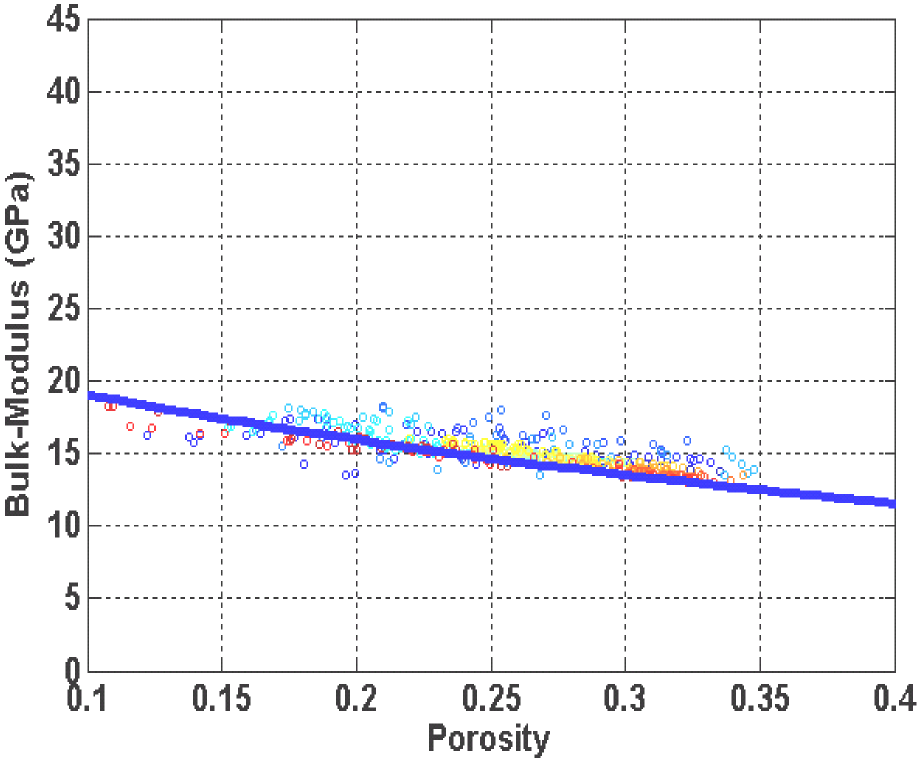

Figure 4-15: Bulk-modulus versus porosity model of TOFTE (Region 2)

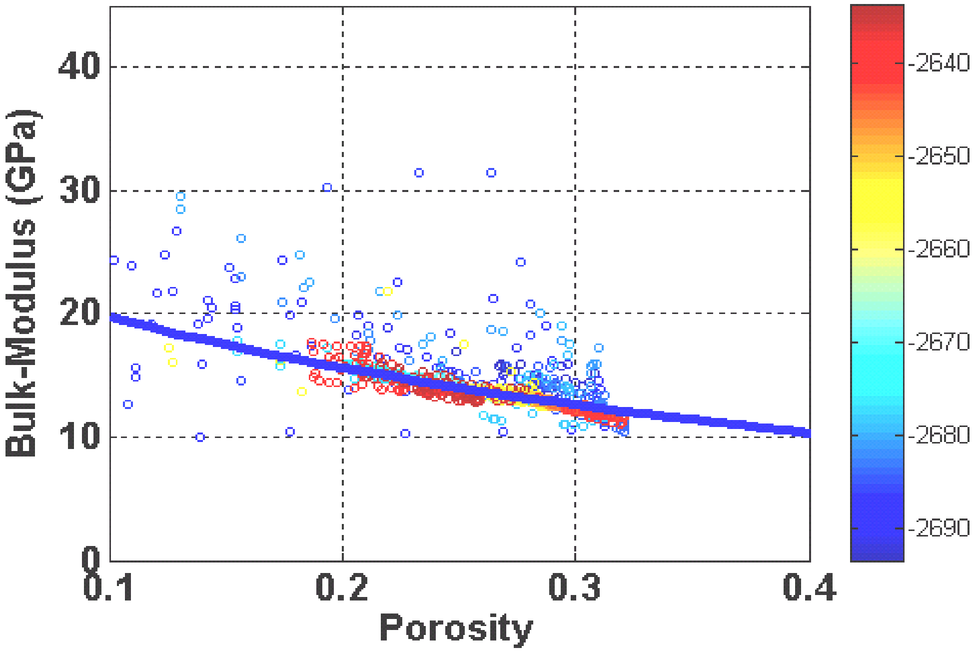

Figure 4-16: Bulk-modulus versus porosity model of TOFTE (Region 3)

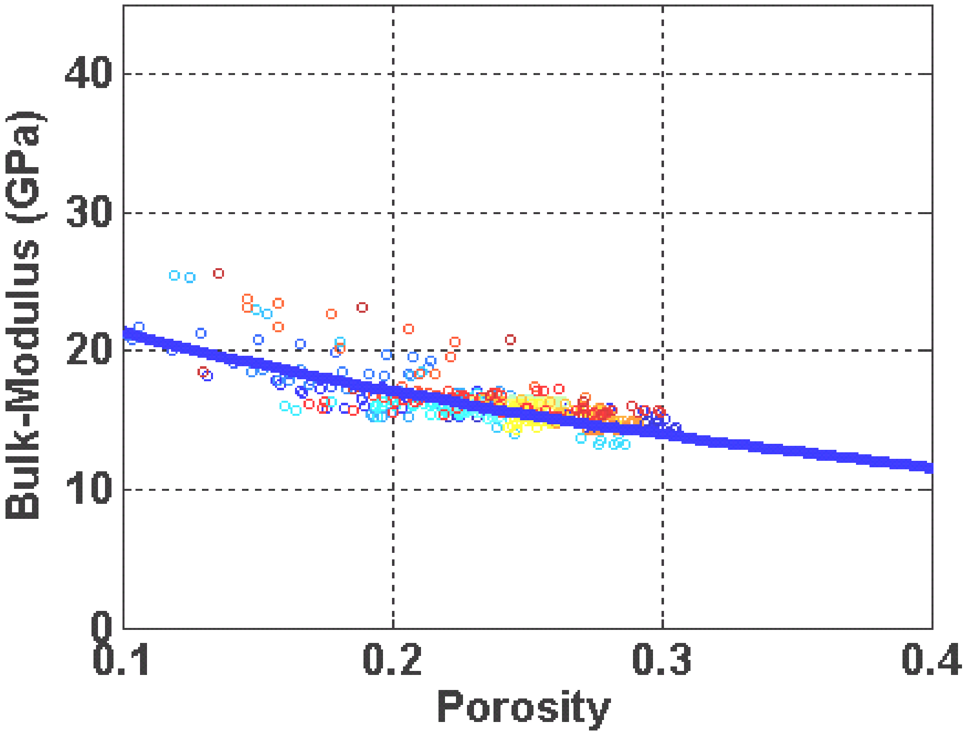

Figure 4-17: Bulk-modulus versus porosity model of TOFTE (Region 4)

4.4.4. ILE Formation

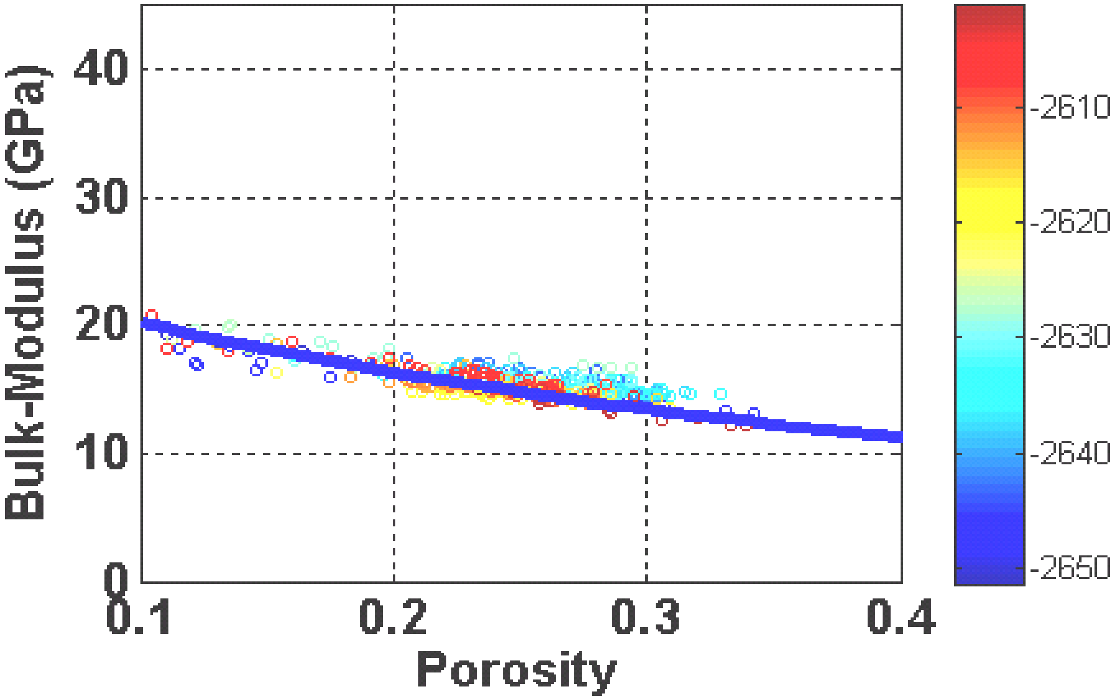

Figure 4-18: Bulk-modulus versus porosity model of ILE (Region 1)

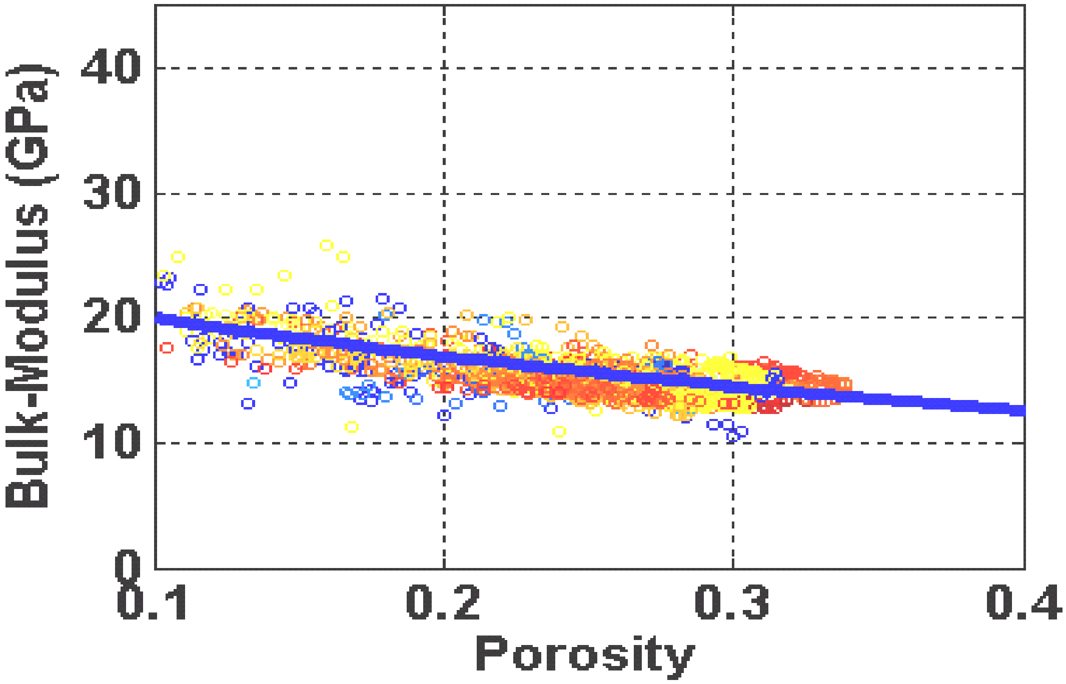

Figure 4-19: Bulk-modulus versus porosity model of ILE (Region 2)

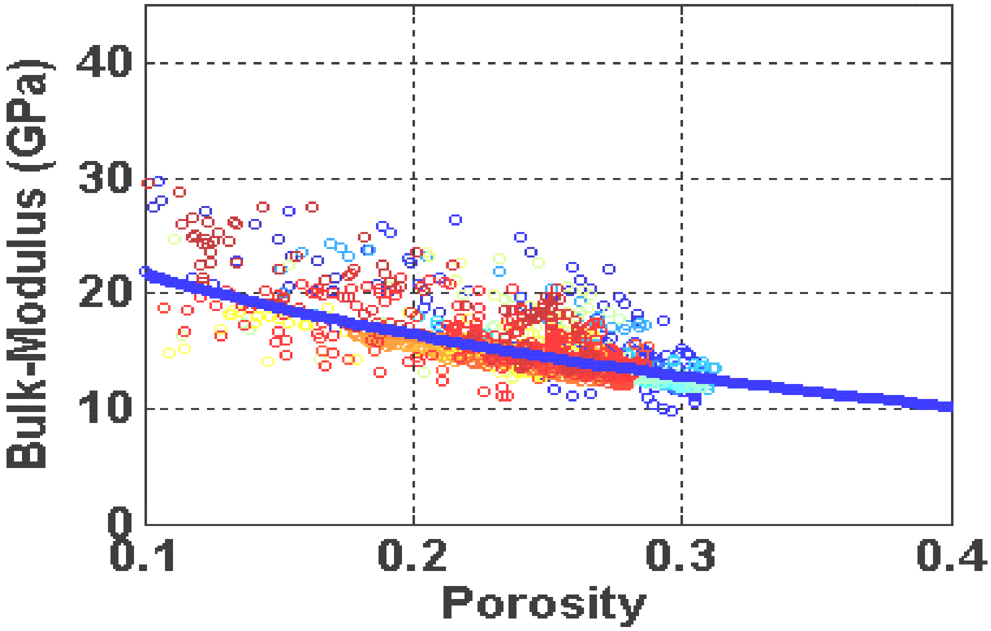

Figure 4-20: Bulk-modulus versus porosity model of ILE (Region 3)

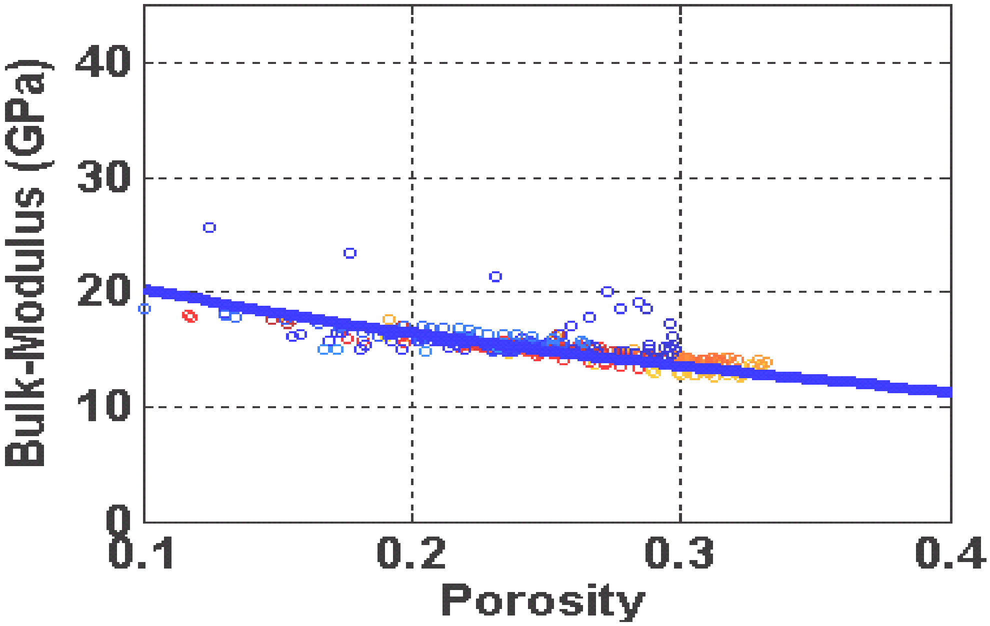

Figure 4-21: Bulk-modulus versus porosity model of ILE (Region 4)

Similarly ILE formation has four clear trends in each of the regions. Figure 4-18, 4-19, 4-20 and 4-21 show models for regions 1, 2, 3 and 4 respectively.

4.4.5. TILJE Formation

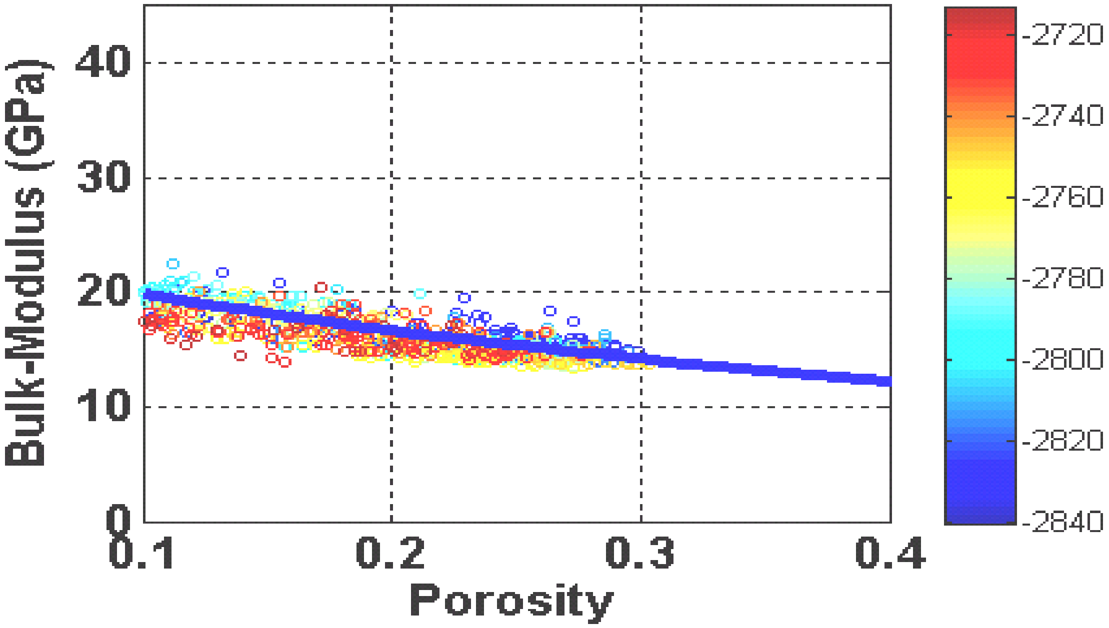

Figure 4-22: Bulk-modulus versus porosity model of TILJE (Region 1)

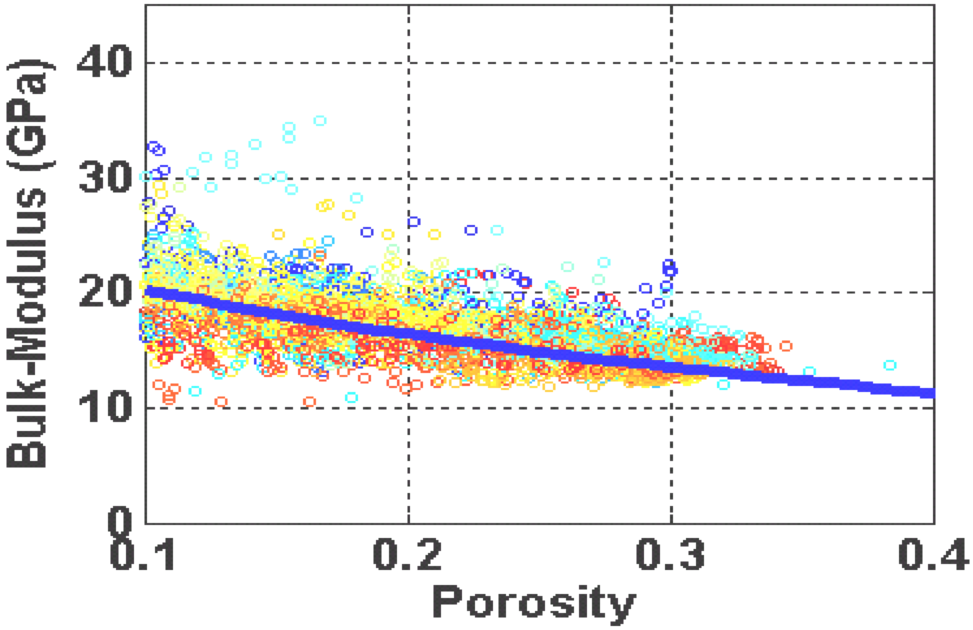

Figure 4-23: Bulk-modulus versus porosity model of TILJE (Region 2)

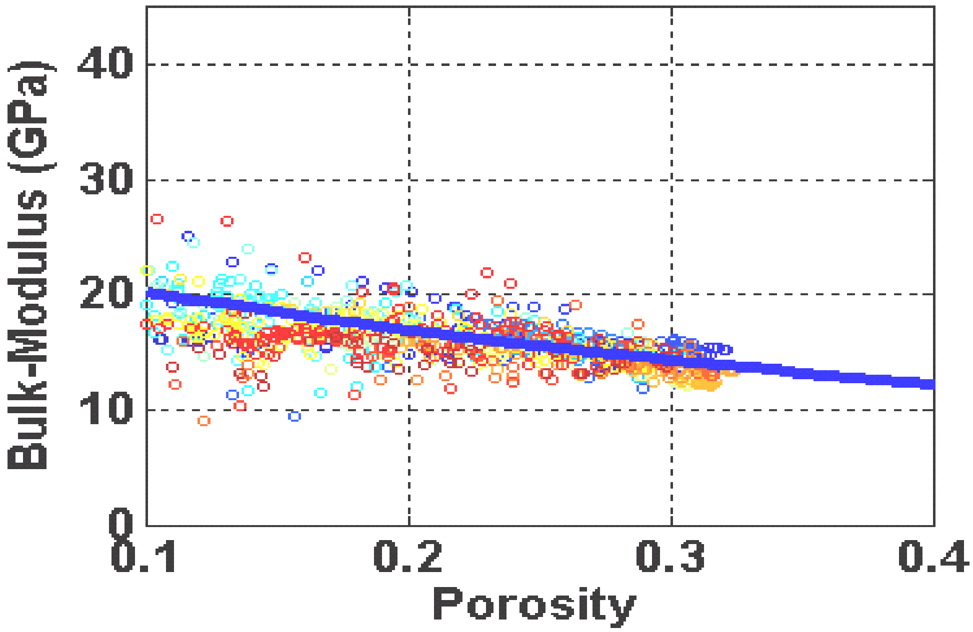

Figure 4-24: Bulk-modulus versus porosity model of TILJE (Region 3)

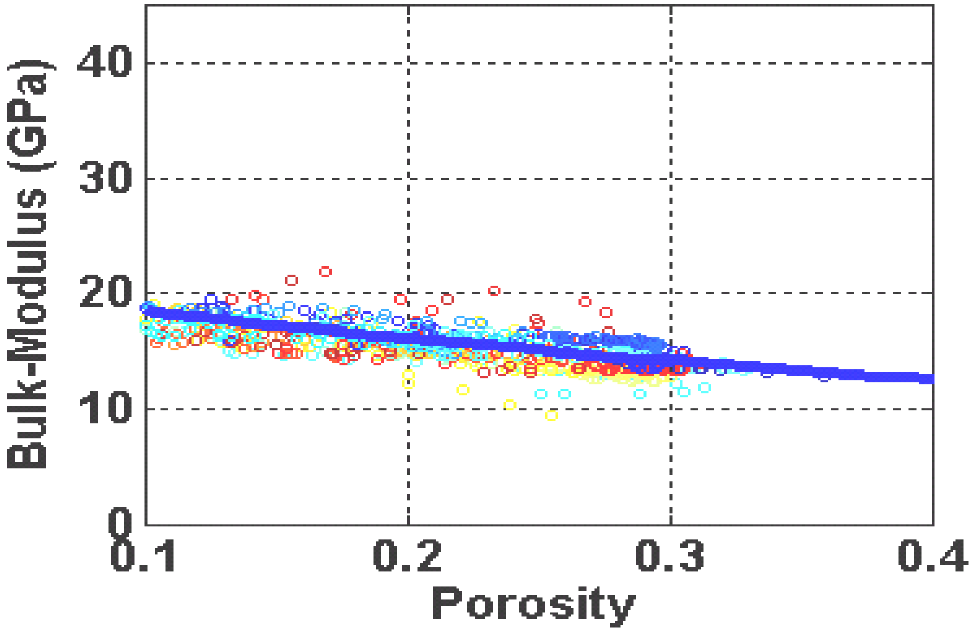

Figure 4-25: Bulk-modulus versus porosity model of TILJE (Region 4)

Similarly figure 4-22, 4-23, 4-24 and 4-25 shows rock physics model for each of the region in TILJE formation. Data points are colored based on their depth. Blue line on the plots represents analytical bulk modulus-porosity model established based on the available data points. V_s for each of the zones is calculated based on the relation between V_P and

V_s, established using well log data. As can be seen from the above plots, careful division of each zone based on the major faults is important to get good rock physics models for elastic moduli versus porosity. The different fault blocks have presumably undergone slightly different amounts of geologic compaction and diagenetic processes, leading to subtle differences in the moduli-porosity trends.

4.5. Flow simulation and time lapse seismic modeling

To generate the 3D seismic velocities (V_p and V_s) at different times during oil production, we performed a flow simulation starting from the initial condition of the reservoir. Flow simulation provided us the distribution of fluids and variation of pore pressure in the reservoir at any particular time and place after the start of production. In order to use Gassmann's equations correctly we need the saturations of each fluid (oil, water and gas) at every point in the model grid at different times. We have used an isothermal black-oil model and flow rates and controls are set up as observed in the field. Thirty years of oil production have been simulated. The general trend in flow simulation is to use one constant pore compressibility for the whole reservoir except in geomechanical studies. So it is difficult to assign pore compressibility for each cell of the reservoir in available flow simulators without considering geomechanics into account. Thus, flow simulation is performed for four different cases to test sensitivity of time-lapse seismic signatures to variations in Cpp. In the first case we have used constant pore compressibility for the whole reservoir as used by original Norne field simulation model (shown in Table 4-1). The next three cases use non-uniform pore compressibility, varying from zone to zone. The second case has different compressibility in each of the zone and it is equal to mean compressibility of the pore compressibility data observed in that zone. The third case uses five percentile of pore compressibility data in each of the zone, while the fourth case has ninty five percentile of pore compressibility data observed in that zone. PVT and capillary pressure data are taken from original Norne field simulation model. Production and injection schedule are as observed in the Norne field.

Cases	**Pore Compressibility**
Case I	Constant (whole reservoir)
Case II	Mean (per zone)
Case III	Five percentile (per zone)
Case IV	Ninty five percentile (per zone)

Table 4 -1: Four different cases for flow simulations

The pressure effect on dry frame velocity is modeled using an analytical curve fit to an empirical relation derived from dry core data for unconsolidated sands (Zimmer et al., 2002) (Figure 4-26).

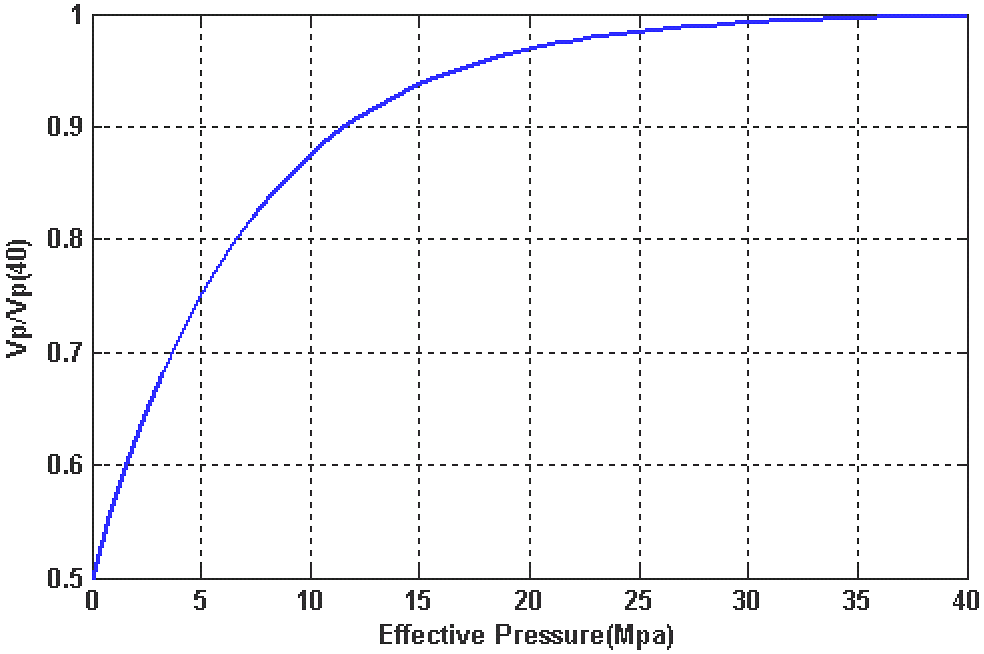

Figure 4-26: Change in seismic velocity due to pore pressure in Norne field

4.6. Results

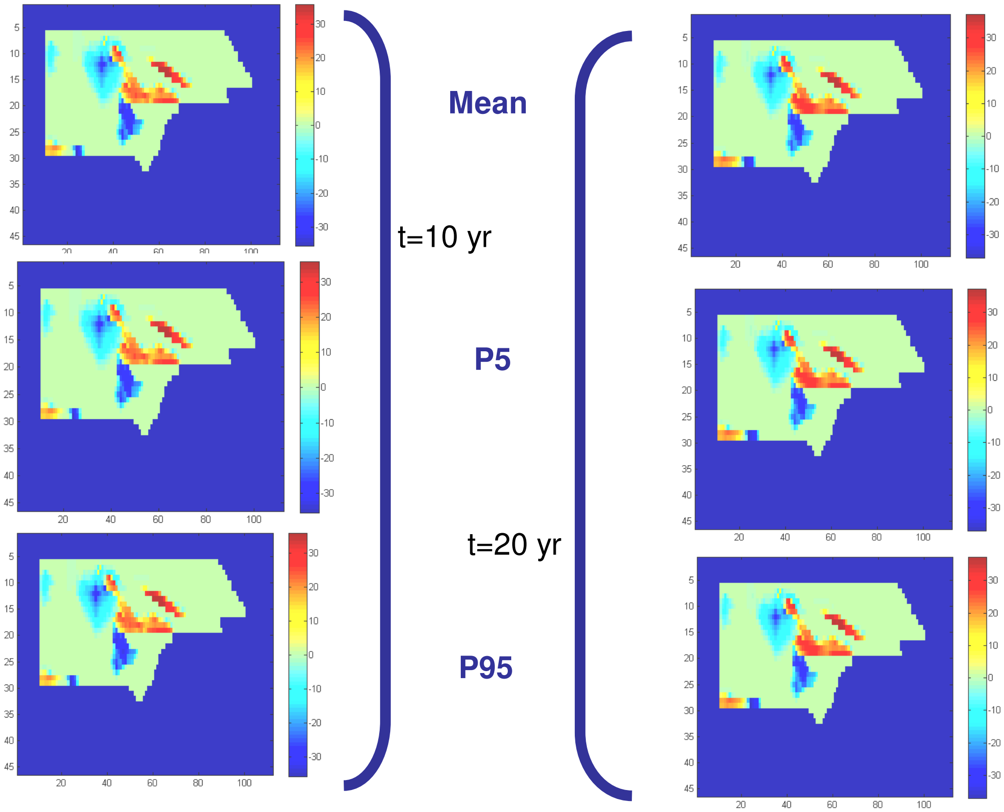

Figure 4-27: Changes in V_P for Case II, III and IV after ten and twenty years

Figure 4-27 shows changes in seismic velocities for a particular layer after ten and twenty years for second, third and fourth case (three cases of simulation run) considering only saturation changes. Here we did not consider effect of pore pressure changes on seismic velocities. From the figure we can infer that changes in seismic velocities for all three sets of pore compressibility are approximately same after ten and twenty years. This indicates that there is no significant change in time lapse seismic modeling for different pore compressibilities *if we consider only saturation changes*.

Next, we considered the effect of change of pore pressure on dry rock frame as well as change of saturation on modeling of seismic velocities. Figure 4-28 describes the criteria for comparison of the results in the above case. We compared change in seismic velocities for different case of flow simulation as stated above (different sets of pore compressibilities).

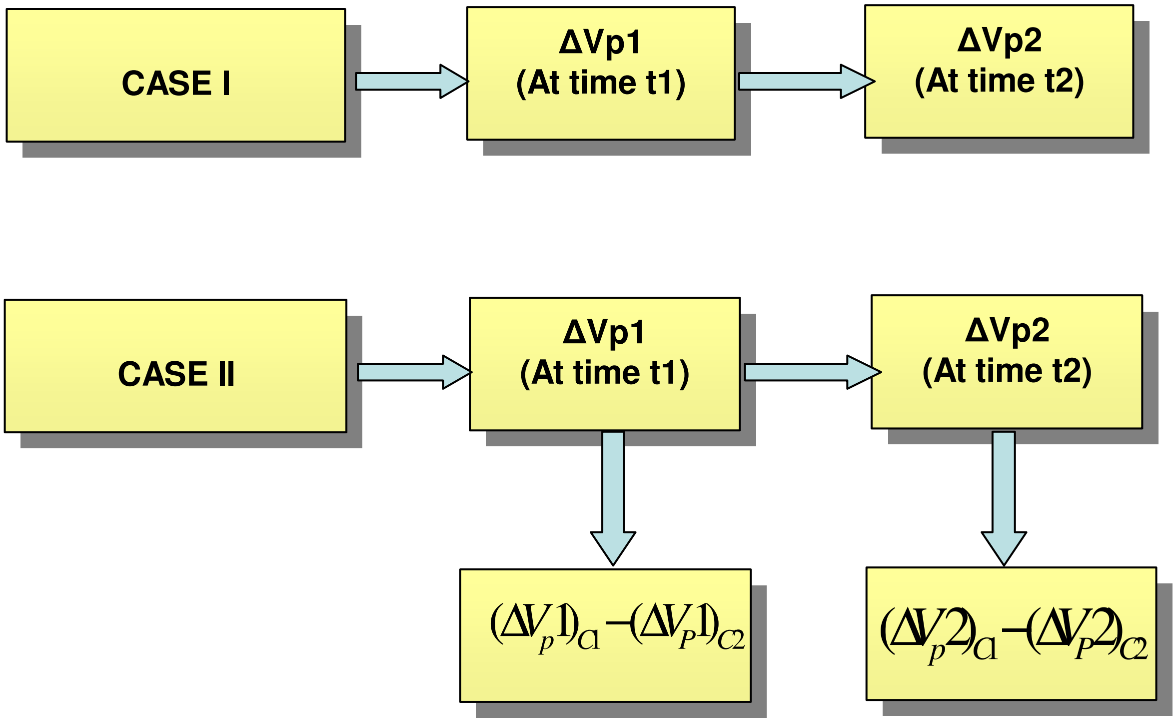

Figure 4-28: Plot defines criteria for comparison of results. We are comparing difference in change of seismic velocities for two different cases and at two different times

Figure 4-29 and 4-30 show difference of change in seismic velocities for Case I and Case III (constant pore compressibility and five percentile pore compressibility) after ten and twenty years respectively. We observed a maximum difference of 27% for the two cases. We also observed spatial variation in seismic velocities for the above two cases.

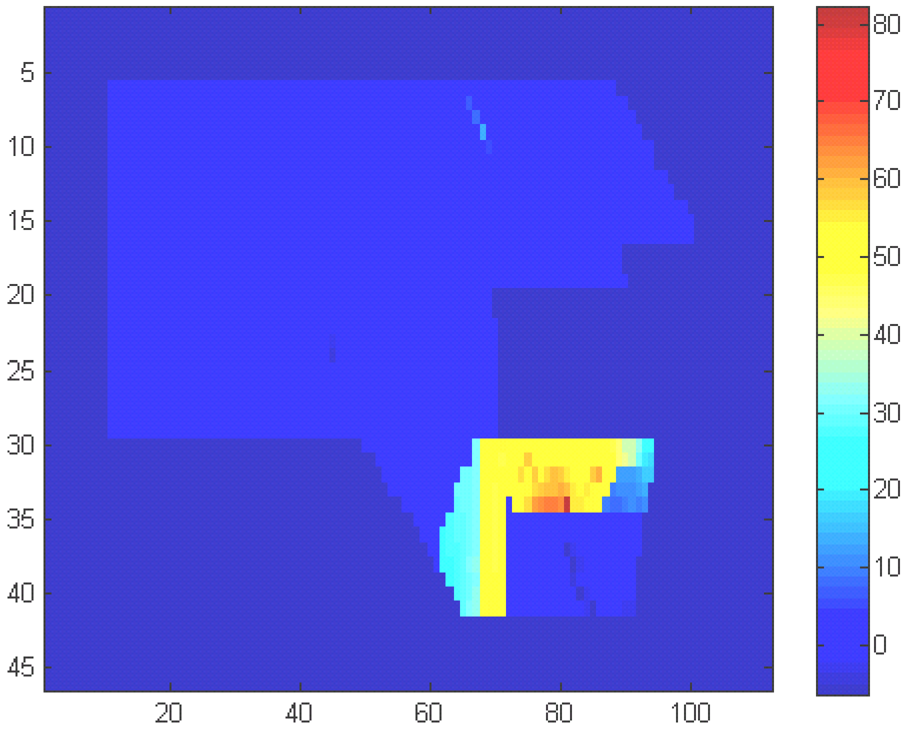

Figure 4-29: $(\Delta V_p 1)_{C1} - (\Delta V_P 1)_{C2}$ after ten years

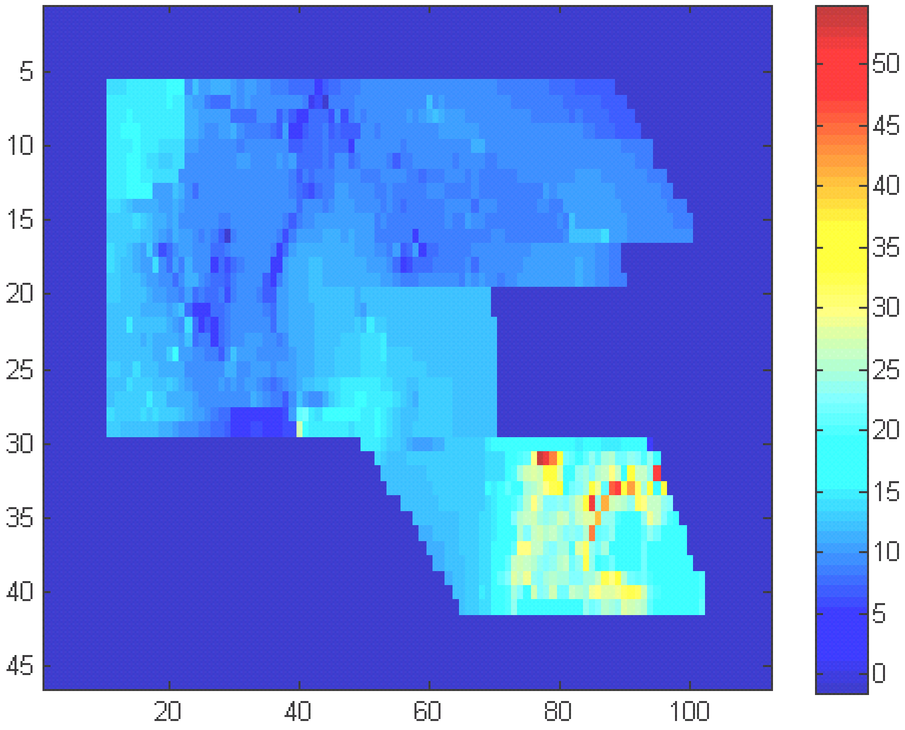

Figure 4-30: $(\Delta V_p 2)_{C1} - (\Delta V_P 2)_{C2}$ after twenty years

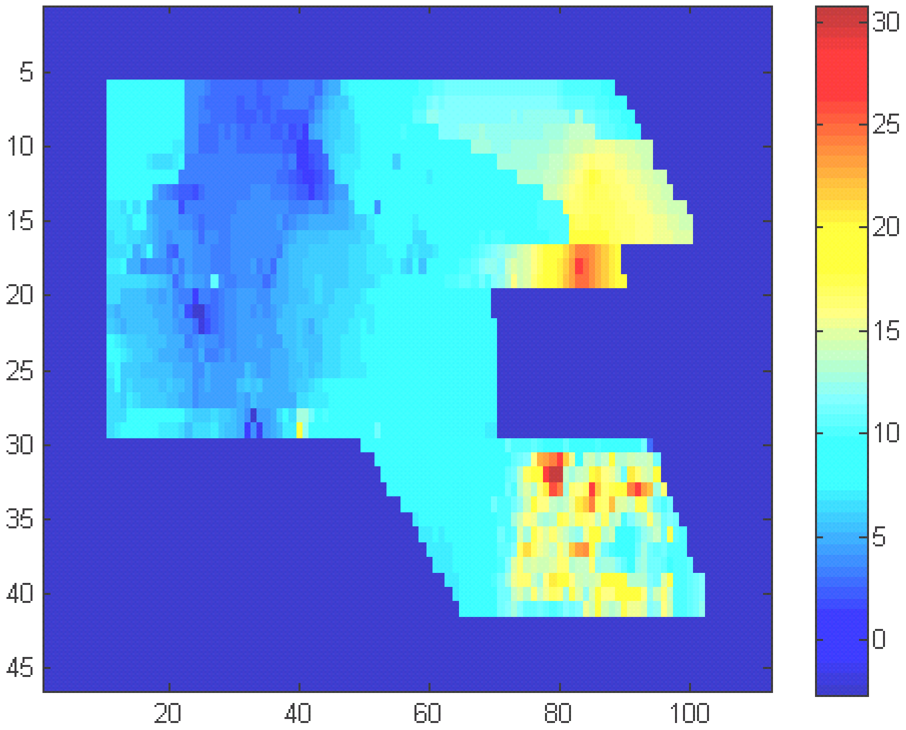

Figure 4-31: $(\Delta V_p 1)_{C1} - (\Delta V_P 1)_{C2}$ after ten years

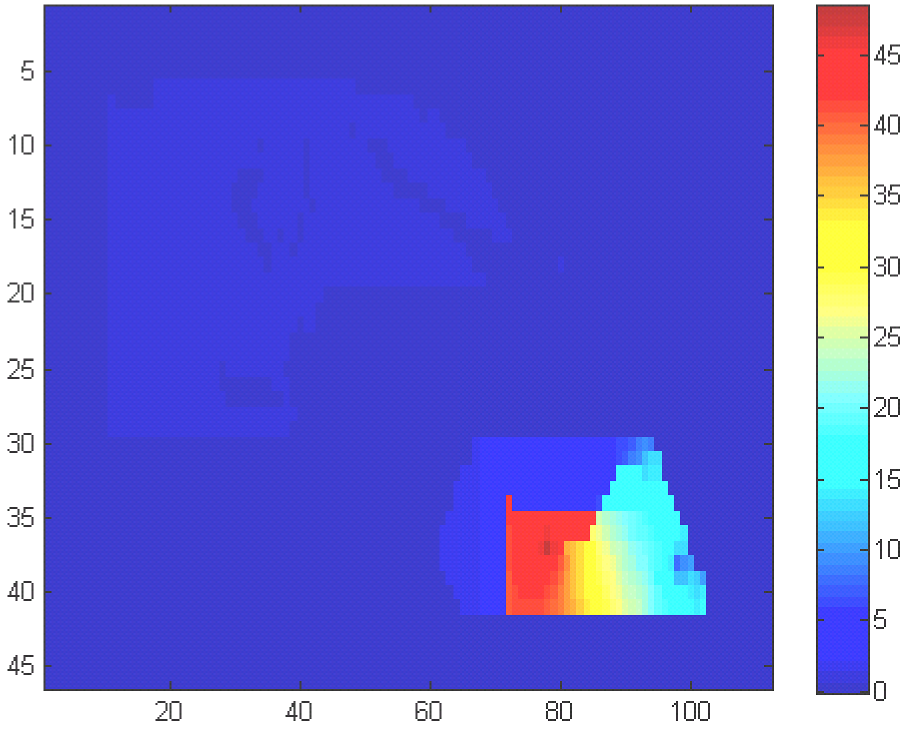

Figure 4-32: $(\Delta V_p 2)_{C1} - (\Delta V_P 2)_{C2}$ after twenty years

Similarly figure 4-31 and 4-32 show the difference in changes in seismic velocities for Case I and Case IV respectively. Here we observe a maximum change of 15 % and 10% after ten and twenty years respectively. Figure 4-33 to 4-36 shows the differences in change of seismic velocities for Case I and Case III (different sets of pore compressibility) at different locations in the reservoir. The red circles are drawn to indicate significant differences for the above two cases.

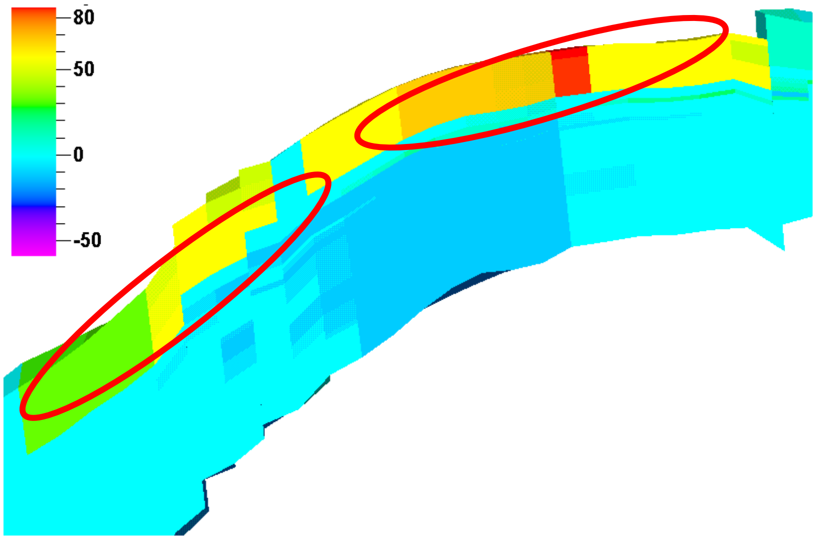

Figure 4-33: Differences in change of seismic velocities for Case I and Case III at different locations in the reservoir.

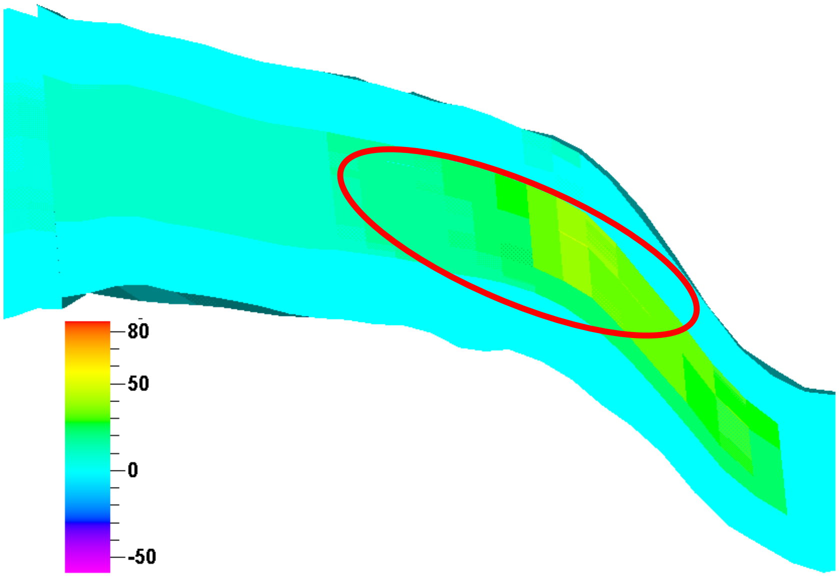

Figure 4-34: Differences in change of seismic velocities for Case I and Case III at different locations in the reservoir.

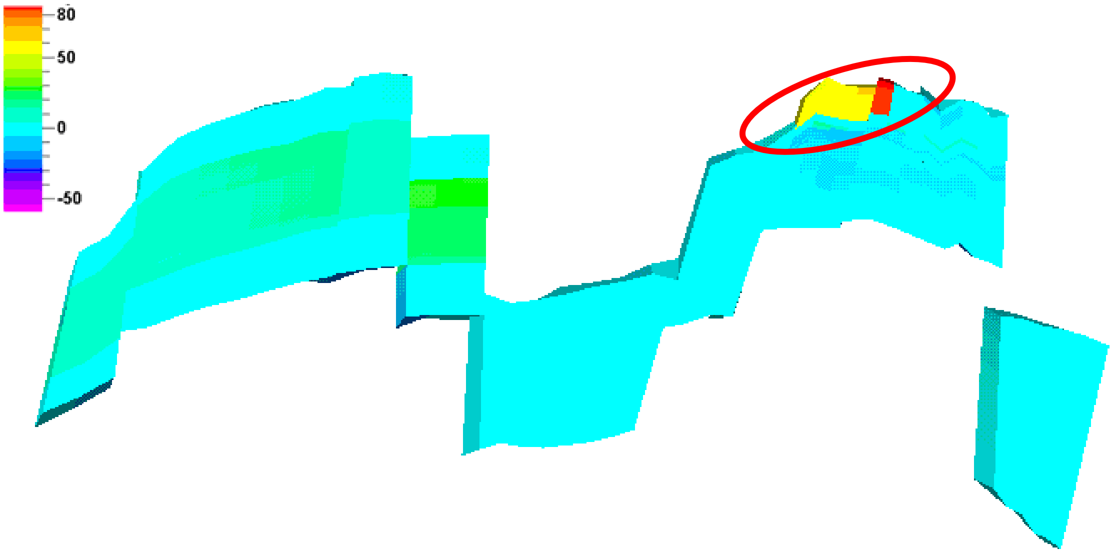

Figure 4-35: Differences in change of seismic velocities for Case I and Case III at different locations in the reservoir.

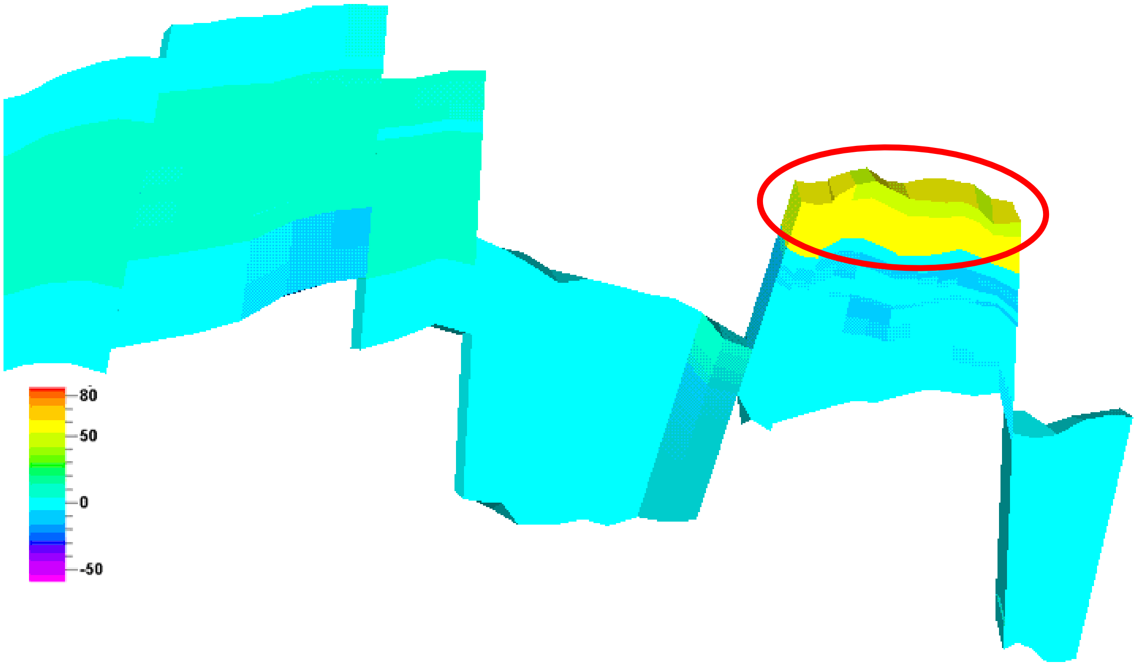

Figure 4-36: Differences in change of seismic velocities for Case I and Case III at different locations in the reservoir.

Chapter 5

5. Conclusions and Future work

In chapter 3 we started with Stanford VI and ran sensitivity on seismic velocities for two different sets of pore compressibility. We observed that for two different pore compressibilities the difference in maximum % change in V_p was around 6%-7%. In addition, the differences were significant as compared to the case where only saturation effects were considered. These observations indicate that production-related changes in seismic velocities can depend upon pore compressibility and thus uncertainties attached to pore compressibilities can not be ignored in time-lapse modeling. Thus, changes in pore pressure and pore compressibility play an important role in time-lapse modeling and hence in seismic history matching. These are very preliminary observations based on a synthetic model, and further analysis on the variation of pore compressibilities, and their relation to different lithologies are done on a real field called Norne.

In chapter 4 we calculated pore compressibility from the available well log data. We observed that pore compressibility varies in each of the zones. Modeling of seismic velocities indicated a maximum difference of 27% for the cases I and case III. We observed a maximum difference of 15% and 10% for case I and Case IV after ten and twenty years respectively. There is also spatial variation in seismic velocities for the above two cases. In time lapse seismic monitoring where changes in time lapse seismic with respect to time is observed, above difference (maximum 27%) is significant and can introduce errors in analysis. We also observed difference in seismic velocities at other locations of the reservoir for two cases. These differences can introduce errors in our analysis during identification of spatial changes in the reservoir using time lapse seismic. Thus it is now clear that uncertainties in pore compressibility can introduce pitfalls in time lapse seismic modeling, especially for reservoirs with pressure-sensitive rocks. These pitfalls would be in both the magnitude of the time-lapse change, and perhaps more importantly, in the spatial patterns of the time lapse changes. It is also clear that using only one pore compressibility for the whole reservoir is not the correct approach for time lapse seismic modeling.

The main purpose of reservoir modeling is better predictions. The general strategy in matching only flow response is to change porosity, permeability or whole reservoir model but often not the pore compressibility. More currently, in seismic history matching, we attempt to optimally constrain our reservoir models to flow response as well as seismic response for better predictions. The above results clearly indicate that while matching flow response as well as seismic response, uncertainties and spatial variability in pore compressibility can play an important role. One of the questions that can arise is that since there are so many uncertainties in reservoir properties, what is the point of introducing one more in pore compressibility? The answer is that although one may be able to reasonably match flow response as well as time-lapse seismic response using a constant pore compressibility for the whole reservoir, it is clear from the examples shown, the predictions may not be accurate not only in terms of quantitative magnitudes but also in terms of qualitative spatial patterns. This is especially important because most often time-lapse seismic data is used qualitatively to asses spatial distributions of production induced changes. Thus uncertainties in pore compressibility can play an important role in optimization of reservoir models based on history matching specially in matching of flow response as well as seismic response.

In future it will be interesting as well as challenging to assign heterogeneous pore compressibility for each cell in the reservoir model. The effect of heterogeneous pore compressibility on flow response as well as seismic response is challenging and should be explored further.

Here we have only modeled seismic velocities. The next step could be modeling of seismic amplitudes. Matching of modeled and observed 4D seismic data should also be explored further.

In a closed loop history matching workflow optimization is generally performed on porosity or permeability. We already observed significance of pore compressibility in time lapse seismic modeling. Variations and optimization of C_{pp} in closed loop history matching workflow will also be interesting to explore.

Nomenclature

σ = Hydrostatic pressure
σ_c = Confining pressure
σ_p = Pore pressure
V_b = Bulk volume
υ_p = Pore volume
C_{bc} = Bulk compressibility of rock
C_{pp} = Pore compressibility of rock
K_{dry} = Dry bulk modulus of rock
μ = Shear modulus of rock
Φ = Porosity
K_{min} = Bulk modulus of the mineral
V_P = Primary seismic velocity
V_S = Secondary seismic velocity
K_{HM} = Effective bulk modulus from Hertz Mindlin theory
G_{HM} = Effective shear modulus from Hertz-Mindlin theory
C = Average number of contacts per grain
υ = Poisson's ratio
K_{fl1} = Bulk modulus of the rock with fluid 1
K_{fl2} = Bulk modulus of the rock with fluid 2
ρ_{fl1} = Density of rock with fluid 1
ρ_{fl2} = Density of rock with fluid 2

References

Avseth, P., Mukerji, T. and Mavko, G. (2005) Quantitative seismic interpretation: applying rock physics tools to reduce interpretation uncertainty, Cambridge University Press

Batzle, M., and Wang, Z., 1992, Seismic properties of pore fluids, Geophysics, 57, 1396-1408.

Castro, S., J. Caers and T. Mukerji, 2005, The Stanford VI Reservoir, Stanford Center for Reservoir Forecasting (SCRF), Annual Report.

Dvorkin, J., and Nur, A., 1996, Elasticity of high-porosity sandstones: Theory for two North Sea datasets, Geophysics, 61, 1363-1370

Gassmann, F., 1951, Über die Elastizität poroser Medien, Vierteljahrsschrift der Naturforschenden Gesellschaft in Zürich, 96, 1-23.

Huang, X., L. Meister, and R. Workman, 1997, Reservoir characterization by integration of time-lapse seismic and production data, SPE Annual Tech. Conf. And Exhibhition.

Huang, X., L. Meister, and R. Workman, 1998, Improving production history matching using time-lapse seismic data, The Leading Edge, October, 1430-1433.

Osdal, B., O. Husby, H. A. Aronsen, N. Chen, and T. Alsos, 2006, Mapping the fluid front and pressure buildup using 4D data on Norne Field: The Leading Edge, 25, 1134–1141.

Steffensen, I. and P. I. Karstad, 1995, Norne field development: Fast track from discovery to production, SPE.

Walker, G. J., and H. S. Lane, 2007, Assessing the accuracy of history-match predictions and the impact of time-lapse seismic data: A case study for the Harding reservoir, SPE 106019.

Zimmer, M., M. Prasad and G. Mavko, 2002, Pressure and porosity influences on VP-VS ratio in unconsolidated sands, SEG expanded abstracts.

Zimmerman, R. W., 1991, Compressibility of Sandstones, Elsevier Science Publishers, Amsterdam, Netherlands.